International Journal of Non–Linear Mechanics 167 (2024) 104868

Contents lists available at ScienceDirect

International Journal of Non-Linear Mechanics

journal homepage: www.elsevier.com/locate/nlm

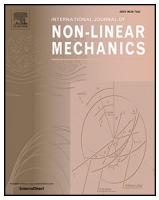

Using differential-algebraic equations and natural coordinates for modelling and simulating cable-driven parallel robots

Giulio Piva, Dario Richiedei *, Alberto Trevisani

Department of Management and Engineering, University of Padova, Stradella San Nicola 3, 36100, Vicenza, Italy

ARTICLE INFO

Keywords:
Cable-driven parallel robots
Dynamic modelling
Numerical simulation
Differential algebraic equations
Natural coordinates

ABSTRACT

This paper proposes a comprehensive approach to the dynamic modelling of Cable-Driven Parallel Robots (CDPRs) by means of Differential-Algebraic Equations (DAEs). CDPRs are usually modelled through a minimal set of Ordinary Differential Equations (ODEs), often by making some simplification or just focusing on the unconstrained platform/end-effector dynamics. The alternative use of redundant DAEs provides several benefits since several non-ideal properties and peculiar operations of CDPRs can be easily and accurately modelled. To provide a comprehensive modelling frame, the typical components of a CDPR with rigid cables are here discussed and modelled by exploiting the concept of DAEs, which use redundant coordinates and embed kinematic constraints in the algebraic part of the equations. Through such advantageous features, it is possible to model swivelling guiding pulleys with non-negligible dimensions and mass. The use of rheonomous constraints is proposed as well, to represent in a simple way the effect of the movable exit-points, that are widely adopted in reconfigurable CDPRs. Finally, the use of Natural Coordinates is proposed for representing spatial end-effectors and modelling some challenging operations such as its overturning or the picking of heavy objects. Numerical simulations and the comparison with the results provided by a benchmark software are shown to demonstrate the accuracy and the computational efficiency of the proposed approach.

1. Introduction

Cable-Driven Parallel Robots (CDPRs) are parallel robots that exploit cables to move an end-effector (EE). Compared to classical parallel robots, CDPRs have larger workspaces, higher dynamic performances, higher payload-to-mass ratios and are easier to reconfigure ([1,2]). On the other hand, their operation is not straightforward since positive and bounded cable tensions must be ensured. Hence, motion planning and control, as well as mechanical design, should properly account for these features of CDPR nonlinear dynamic behaviour ([1–4]), which makes the availability of accurate dynamic models a basic goal.

Following the typical approach used for traditional parallel robots (see e.g., Ref. [4]), dynamic models of CDPRs are commonly formulated through the Newton-Euler equations that directly lead to a minimal set of Ordinary Differential Equations (ODEs) (see e.g., Refs. [1,5–10]). Their formulation is straightforward if just the EE is considered and is treated as an unconstrained rigid body excited by cable tensions and external forces (generating the so-called external wrench); however, equation complexity considerably rises when trying to consider motor dynamics and other non-ideal or nonlinear dynamical terms such as swivel angles or movable cable exit-points (EPs).

An alternative approach is using redundant Differential-Algebraic Equations (DAEs). DAEs are widely adopted to model multibody systems for easily handling the constrained dynamics, but have been occasionally used to model CDPRs ([11–16]), usually just to include motor dynamics. The benefits of DAEs compared to ODEs, have been widely discussed in multibody dynamic modelling, and in general, they can be summarized as follows: 1) DAEs allow the systematic assembly of open and closed chain multibody systems, 2) the resulting equation can be solved using several effective and efficient state-of-the-art solution schemes and integrators, 3) DAEs can be directly connected to nonlinear finite element formulations. When employed to model CDPRs, DAEs also have the advantage of easily representing some peculiar features that are difficult to model by ODEs, thanks to the redundant coordinates. The benefit of DAEs and redundant coordinates can be extended if natural coordinates (NCs) are adopted ([16–18]). NCs include the Cartesian coordinates of some points together with the Cartesian components of some unit vectors. The primary advantage of NCs is that they do not exploit angles or angular parameters to define orientation, which leads to constant mass matrices and to simple constraint equations. Another advantage related to NCs, which is relevant for CDPRs, is the absence of

* Corresponding author.
E-mail addresses: giulio.piva@phd.unipd.it (G. Piva), dario.richiedei@unipd.it (D. Richiedei), alberto.trevisani@unipd.it (A. Trevisani).

https://doi.org/10.1016/j.ijnonlinmec.2024.104868
Received 1 August 2023; Received in revised form 22 July 2024; Accepted 5 August 2024
Available online 8 August 2024

Nomenclature

A_i = *i-th* EP
α_p, ξ_p, ω_p = Parameters of the "penalty formulation"
$\mathbf{a}$ = Vector of parameters describing the position of the CM of the EE with respect to the local reference frame
$\mathbf{a}_i$ = Vector of Cartesian coordinates describing the absolute position of the *i-th* EP
B_i = *i-th* anchor point
$\mathbf{b}_i$, $\overline{\mathbf{b}}_i$ = Vectors of the absolute and local Cartesian coordinates of the *i-th* anchor point
$\mathbf{C}_p$ = Matrix related to point $\mathbf{p}$ projecting the natural coordinates in the three-dimensional Cartesian space
χ_1,χ_2,χ_3 = angular parameters exploited for representing the rigid connection between two rigid bodies
$\mathbf{c}$ = Vector encompassing the components of the local position of a point with respect to the basic point $\mathbf{r}_i$
D_i = Point exploited in the swivel pulley's formulation
$\boldsymbol{\delta}_i$ = Vector connecting the *i-th* anchor point to the point of rotation of the *i-th* guiding pulley
$\mathbf{d}_i$ = Vector of Cartesian coordinates describing the absolute position of D_i
E = Origin of the body fixed local reference frame
$\boldsymbol{\varepsilon}$, $\overline{\boldsymbol{\varepsilon}}$ = Minimal coordinates used to describe the EE pose and absolute velocity
$\boldsymbol{\varphi}$ = Set of parameters exploited in the minimal parametrization of the rotation of the EE
Φ_1,ϕ_2,ϕ_3 = Angular parameters exploited in the Natural Coordinates Formulation
$\boldsymbol{\Phi}, \dot{\boldsymbol{\Phi}}, \ddot{\boldsymbol{\Phi}}$ = Set of algebraic constraints at position, velocity and acceleration level
$\boldsymbol{\Phi}_{/\mathbf{t}}$ = Matrix of partial derivatives of $\boldsymbol{\Phi}$ with respect to the generic set $\mathbf{t}$
f_i = Modulus of tension on the *i-th* cable
$\mathbf{f}$ = Vector of external forces
$\mathbf{f}_c$ = Vector of reaction forces arising from the kinematic constraints
$\boldsymbol{\gamma}$ = Vector of components arising from the algebraic constrains at the acceleration level
$\mathbf{H}(\boldsymbol{\varphi})$ = Projection matrix exploited to compute the absolute angular velocity of the EE
$\mathbf{I}_{n\times n}$ = Identity matrix of dimension $n \times n$
$J_{m,i}$ = Moment of inertia of the *i-th* motor
J_{pulley} = Moment of inertia of the swivel pulley
$\mathbf{J}$ = Inertia tensor of a rigid body
$\boldsymbol{\lambda}$ = Lagrange multiplier vector
l_i = Length of the *i-th* cable
$\mathbf{M}$ = CDPR mass matrix
m_{ee} = Mass of the EE
$n_{\mathbf{t}}$ = Number of elements of generic set $\mathbf{t}$
$\mathbf{n}_i$ = Unit vector exploited in the swivel pulley formulation
O = Origin of the global reference frame
ψ_i = Angle involved in the swivel pulley formulation
$\mathbf{p}$ = Vector of Cartesian coordinates of EE absolute position
$\mathbf{q}, \dot{\mathbf{q}}, \ddot{\mathbf{q}}$ = Dependent coordinates at the position, velocity and acceleration level
r_i = Radius of the *i-th* winch coiling the cable
$\widetilde{r}$ = Radius of the guiding pulley
$\mathbf{r}$ = Vector of Cartesian coordinates used to describe the absolute position of a basic point of the Natural Coordinate Formulation
σ_i = Swivel angle of the *i-th* guiding pulley
$\mathbf{s}_i$ = Unit vector starting from $\mathbf{d}_i$ and directed to the center of the guiding pulley
$\theta, \dot{\theta}, \ddot{\theta}$ = Angular position, velocity and acceleration of a motor
$\mathbf{u}$ = Unit vector describing the direction of a cable tension
$\mathbf{v}$ = Unit vector exploited in the Natural Coordinate Formulation
$\mathbf{w}_e$ = Vector of external actions exerted on the EE
$\mathbf{X}$ = Matrix exploited to represent the global orientation of a rigid body described through natural coordinates
$\mathbf{Z}$ = Matrix projecting the inertia tensor of a rigid body on the natural coordinates
$\mathbf{z}$ = Vector of independent coordinates
$\boldsymbol{\omega}$ = Angular velocity of the EE

singularities of the transformation matrix, which are instead experienced by several rigid-body representations ([19]). As a consequence, NCs are suitable to represent very challenging operations, such as the overturning of the EE, and the on-the-fly joining between the EE and an object to be transported, since no barycentric coordinates are required: indeed, the change in the position of the centre of mass of the EE cannot be neglected when dealing with transport operations but is difficult to handle through traditional coordinate representations used in robotics.

By highlighting these peculiar and advantageous features of DAEs and NCs, this paper introduces and discusses their use in CDPR modelling and simulations, paying particular attention to the practical and numerical issues related to CDPRs. As a result, a comprehensive approach is devised, which also introduces some novel formulations, thus enlarging the use of DAEs in the field of CDPRs compared with the existing literature. In detail, the following topics are covered by the paper.

- The general model formulation through DAEs for CDPRs with rigid cable is outlined in Section 2.
- The representation of 6-DOF EEs through NCs is proposed in Section 3, where the picking of a load is discussed too.
- The inclusion of motors and swivel guiding pulleys is discussed in Section 4, by also handling pulleys with non-negligible dimension (and hence variable EP) and non-negligible inertia.
- The representation of movable cable EPs, as those often used in reconfigurable CDPRs ([20,21]), is proposed in Section 5, by exploiting the concept of rheonomous constraints, thus avoiding the dynamic modelling of the subsystems used to drive such points.

Numerical assessments are provided through several examples, by also comparing the results with those sported by the benchmark software MSC ADAMS.

2. General Index-3 formulation of the DAE model

The modelling approach proposed in this paper relies on formulating the model as a set of DAEs with differential index equal to 3:

$$\begin{cases} \mathbf{M}\ddot{\mathbf{q}} + \boldsymbol{\Phi}_{/\mathbf{q}}^{T}\boldsymbol{\lambda} = \mathbf{f} \\ \boldsymbol{\Phi}(\mathbf{q}, t) = \mathbf{0} \end{cases} \tag{1}$$

The CDPR is described through a set of n_q generalized (redundant) coordinates $\mathbf{q} \in \mathbb{R}^{n_q}$, related by n_Φ linearly independent, holonomic kinematic constraints $\boldsymbol{\Phi}(\mathbf{q}, t) \in \mathbb{R}^{n_\Phi}$, and including both the coordinates of the EE and the motor rotations (and of the guiding pulleys whenever necessary). The dependence on time vanishes if all the constraints are scleronomous. $\boldsymbol{\Phi}$ will include the constraints due to cables, collected in $\boldsymbol{\Phi}_c$ and the rigid-body constraints required whenever natural

coordinates are adopted to model a spatial EE, that are collected within $\mathbf{\Phi}_{rbc}$ (see Section 3.3)

The number of degrees of freedom (DOF) of the system is therefore $n_{DOF} = n_q - n_\Phi$. $\mathbf{\Phi}_{\mathbf{q}} = \left[\frac{\partial \mathbf{\Phi}}{\partial \mathbf{q}}\right] \in \mathbb{R}^{n_\Phi \times n_q}$ is the Jacobian matrix of the constraints, and $\boldsymbol{\lambda} \in \mathbb{R}^{n_\Phi}$ is the vector of Lagrange multipliers. All the external forces applied to the overall system are collected in vector $\mathbf{f} \in \mathbb{R}^{n_q}$ together with all the velocity-dependent forces (if present). The reaction forces introduced by the kinematic constraints, $\mathbf{f}_c \in \mathbb{R}^{n_q}$, are represented through $\mathbf{\Phi}_{\mathbf{q}}^T \boldsymbol{\lambda} \in \mathbb{R}^{n_q}$, also including cable tensions. Finally, $\mathbf{M} \in \mathbb{R}^{n_q \times n_q}$ is the mass matrix: a wise choice of $\mathbf{q}$ makes constant such a matrix, and hence Coriolis and centripetal terms in $\mathbf{f}$ vanish (see Ref. [24] and Section 3.3).

By assuming massless and inextensible cables with a point-like representation of the exit-point (EP) (see Section 4), the *i-th* cable ($i = 1,\ldots, n_c$, with n_c denoting the number of cables) is represented within $\mathbf{\Phi}_c$, through the following algebraic constraint

$$\Phi_{c,i} = (\mathbf{b}_i - \mathbf{a}_i)^T (\mathbf{b}_i - \mathbf{a}_i) - l_i^2 = 0 \tag{2}$$

l_i is the length of the cable, and it is linked to the angular position of the motor θ_i by means of the radius of the winch that coils the cable r_i ($l_{0,i}$ is the cable length corresponding to $\theta_i = 0$):

$$l_i = l_{0,i} + r_i \theta_i \tag{3}$$

$\mathbf{b}_i \in \mathbb{R}^3$ denotes the absolute position of the *i-th* anchor point B_i (i.e., the point of the EE connected to the *i-th* cable), while $\mathbf{a}_i \in \mathbb{R}^3$ denotes the position of the *i-th* EP A_i. More details can be found in Section 4.

The forces arising from the kinematic constraints related to the cables, i.e., the cable tensions, are represented in the differential part of the DAEs through the Lagrange multipliers. Details on tension computation are provided in Appendix A.

The overall number of constraints is related to the choice of $\mathbf{q}$, and to the physical properties of the CDPR. Section 3.3 discusses how to choose $\mathbf{q}$ and then how to formulate $\mathbf{M}$ and $\mathbf{\Phi}$ in accordance with the features of the main components of a CDPR.

Formulating complex dynamic models with DAE has been widely shown that is easier, thanks to using redundant coordinates and incorporating the algebraic constraints. Then, the numerical solution of such DAEs for forward dynamics usually exploit transformations to ODEs, by means of some well-established methods [16] and the resulting ODEs can be numerically integrated to solve the forward dynamics, by exploiting the efficient approaches proposed in the literature ([18]).

In particular, the use of either the penalty formulation and method based on the index-1 DAE formulation (such as the Udwadia-Kalaba method, see Ref. [16] for an overview) that leads to ODEs with redundant coordinates, allow easily solving models of overactuated (over-constrained) systems, without requiring the complex algebraic manipulations required by ODE-based models and allowing for accurate calculations of the cable tensions. This is another advantage of DAE-based formulations.

3. Modelling of the EE

3.1. 3-Dimensional lumped EE

When the EE has negligible dimensions, it can be modelled as a lumped mass, m_{ee}, whose motion is described by three absolute Cartesian displacements, $\mathbf{p} \in \mathbb{R}^3$ ([3,22]). The EE contributes on $\mathbf{M}$ is through the following constant submatrix:

$$\mathbf{M}_{ee} = \begin{bmatrix} m_{ee} & 0 & 0 \\ 0 & m_{ee} & 0 \\ 0 & 0 & m_{ee} \end{bmatrix} \tag{4}$$

3.2. 6-Dimensional EE modelled through minimal coordinates

Six DOFs are assumed if the EE dimensions cannot be neglected. By following the typical approach of robotics, the minimal representation exploits three absolute Cartesian positions, $\mathbf{p}$, and three rotational coordinates $\boldsymbol{\varphi}$ that describe the origin and orientation of the body-fixed coordinate system with respect to the global frame, leading to the coordinate vector $\boldsymbol{\varepsilon} = \begin{bmatrix} \mathbf{p}^T & \boldsymbol{\varphi}^T \end{bmatrix}^T$. Several definitions of $\boldsymbol{\varphi}$ can be adopted, such as, for example, the Euler angles, the Euler/Rodrigues parameters [19]. The absolute velocity of the EE, $\dot{\bar{\boldsymbol{\varepsilon}}} = \begin{bmatrix} \dot{\mathbf{p}}^T & \boldsymbol{\omega}^T \end{bmatrix}^T$, includes the translational velocities, $\dot{\mathbf{p}}$, and the angular velocity vector $\boldsymbol{\omega}$, that are "quasi-coordinates" that exist only as differentials. By means of the kinematic differential transformation $\dot{\boldsymbol{\varphi}} = \mathbf{H}(\boldsymbol{\varphi})\boldsymbol{\omega}$ (where the formulation of $\mathbf{H}$ is related to the definition assumed for the angles), the coordinate vector at the velocity level can be obtained.

The equations of motion of the unconstrained subsystem made by the EE are expressed as

$$\mathbf{M}_{ee}(\boldsymbol{\varepsilon})\ddot{\bar{\boldsymbol{\varepsilon}}} = \mathbf{f}_{ee} \tag{5}$$

where $\mathbf{f}_{ee}$ includes the external forces applied to the EE (the so-called external wrench), as well as Coriolis and centripetal terms caused to the pose-dependent, non-constant mass matrix $\mathbf{M}_{ee}(\boldsymbol{\varepsilon})$ ([23,24]), and the effect of the cable tensions on the platform through the so-called structure matrix.

The drawback of such a representation is that the non-constant projection matrix $\mathbf{H}(\boldsymbol{\varphi})$ becomes singular for some values of $\boldsymbol{\varphi}$. Therefore, large rotation of the EE, such as overturning or singular configurations leading to a gimbal lock, cannot be represented.

3.3. 6-Dimensional EE modelled through natural coordinates

An effective technique that overcomes the problems arising from a minimal coordinates representation is the Natural Coordinates Formulation (NCF) ([17,18,25–27]), that simplifies modelling of multibody systems. Such a formulation represents a spatial rigid body through points and unit vectors, the so-called natural coordinates (NCs): a proper choice of the natural coordinates leads to a constant mass matrix of the body, $\mathbf{M}_{ee}$, and therefore no Coriolis and centripetal forces appear in Eq. (1) ([24]). Additionally, this choice of coordinates does not experience singularities.

The usual definition of the vector of NCs for a spatial body, $\mathbf{q}_{nc} \in \mathbb{R}^{12}$, is based on two points, defined through their absolute position vectors $\mathbf{r}_i$, $\mathbf{r}_j \in \mathbb{R}^3$, and two non-coplanar unit-vectors $\mathbf{v}_i, \mathbf{v}_j \in \mathbb{R}^3$ ([18]), (see Fig. 1) defined with respect to the global reference frame $\mathrm{O}_{\mathbf{xyz}}$:

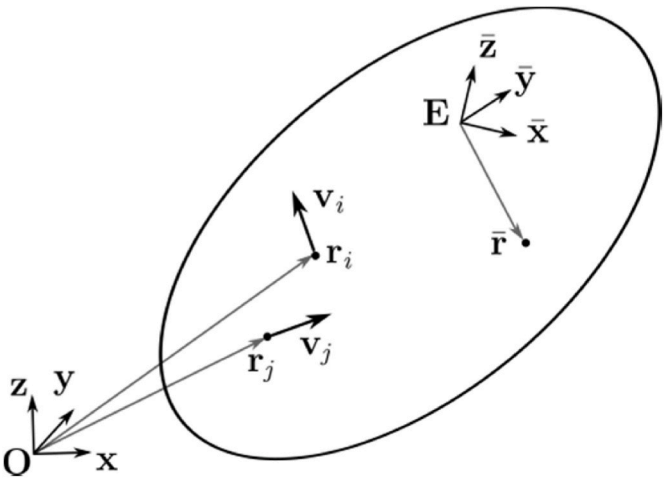

Fig. 1. Rigid body described through NCs.

$$\mathbf{q}_{nc} = \begin{bmatrix} \mathbf{r}_i^T & \mathbf{r}_j^T & \mathbf{v}_i^T & \mathbf{v}_j^T \end{bmatrix}^T \tag{6}$$

The NCs can be arranged into a full rank matrix:

$$\mathbf{X} = \begin{bmatrix} (\mathbf{r}_j - \mathbf{r}_i) & \mathbf{v}_i & \mathbf{v}_j \end{bmatrix} \in \mathbb{R}^{3\times 3} \tag{7}$$

and its counterpart expressed with respect to the local reference frame $E_{\overline{xyz}}$:

$$\overline{\mathbf{X}} = \begin{bmatrix} (\overline{\mathbf{r}}_j - \overline{\mathbf{r}}_i) & \overline{\mathbf{v}}_i & \overline{\mathbf{v}}_j \end{bmatrix} \tag{8}$$

This matrix encompasses the triplet that defines three directions associated to the $\mathbf{q}_{nc}$ and can be used to retrieve the global orientation of the body and its angular velocity ([27]), $\boldsymbol{\omega} = \dot{\mathbf{X}}\mathbf{X}^{-1}$:

3.3.1. Mass matrix

The following developments are taken from ([23]); here, just the main results are proposed. The mass matrix $\mathbf{M} \in \mathbb{R}^{12\times 12}$ for a spatial body defined through the twelve coordinates $\mathbf{q}_{nc}$ is the following constant matrix:

$$\mathbf{M}_{nc} = \begin{bmatrix} (m - 2ma_1 + z_{11})\mathbf{I}_{3\times 3} & (ma_1 - z_{11})\mathbf{I}_{3\times 3} & (ma_2 - z_{12})\mathbf{I}_{3\times 3} & (ma_3 - z_{13})\mathbf{I}_{3\times 3} \\ (ma_1 - z_{11})\mathbf{I}_{3\times 3} & z_{11}\mathbf{I}_{3\times 3} & z_{12}\mathbf{I}_{3\times 3} & z_{13}\mathbf{I}_{3\times 3} \\ (ma_2 - z_{21})\mathbf{I}_{3\times 3} & z_{21}\mathbf{I}_{3\times 3} & z_{22}\mathbf{I}_{3\times 3} & z_{23}\mathbf{I}_{3\times 3} \\ (ma_3 - z_{31})\mathbf{I}_{3\times 3} & z_{31}\mathbf{I}_{3\times 3} & z_{32}\mathbf{I}_{3\times 3} & z_{33}\mathbf{I}_{3\times 3} \end{bmatrix} \tag{9}$$

$m = \int_\Omega \rho d\Omega$ denotes the overall mass of the body (Ω is the body volume).

The scalars a_r and z_{kh} (for arbitrary indexes r, k, h) denote entries of vector $\mathbf{a}$ (related to the position of the center of mass (CM) in the moving reference $\overline{\mathbf{r}}_{CM}$) and of matrix $\mathbf{Z}$ (related with the inertia tensor $\mathbf{J}_i$), and are given by the following:

$$\mathbf{a} = \overline{\mathbf{X}}^{-1}(\overline{\mathbf{r}}_{CM} - \overline{\mathbf{r}}_i) \tag{10}$$

$$\mathbf{Z} = \overline{\mathbf{X}}^{-1}\mathbf{J}_i\overline{\mathbf{X}}^{-T} \tag{11}$$

The inertia tensor of the NCF, $\mathbf{J}_i$, is related to the "standard one" used in Euler equations, $\mathbf{J}_{CM}$:

$$\mathbf{J}_{CM} = \int_\Omega \begin{bmatrix} \overline{r}_y^2 + \overline{r}_z^2 & -\overline{r}_x\overline{r}_y & -\overline{r}_x\overline{r}_z \\ -\overline{r}_y\overline{r}_x & \overline{r}_z^2 + \overline{r}_x^2 & -\overline{r}_y\overline{r}_z \\ -\overline{r}_z\overline{r}_x & -\overline{r}_z\overline{r}_y & \overline{r}_x^2 + \overline{r}_y^2 \end{bmatrix} dm \tag{12}$$

by means of the following expression:

$$\mathbf{J}_i = \frac{1}{2}\mathbf{I}_{3\times 3}\mathrm{trace}(\mathbf{J}_{CM}) - \mathbf{J}_{CM} + m(\overline{\mathbf{r}}_{CM} - \overline{\mathbf{r}}_i)(\overline{\mathbf{r}}_{CM} - \overline{\mathbf{r}}_i)^T \tag{13}$$

3.3.2. Constraints

The rigid body conditions that need to be ensured are expressed as six kinematic constraints which should be defined between the NCs to ensure the rigid body condition, leading to the set of holonomic, scleronomous constraints $\boldsymbol{\Phi}_{rbc} \in \mathbb{R}^6$. A distance constraint (the first one in Eq. (14)) is defined to impose the constant distance between two basic points $\mathbf{r}_i$ and $\mathbf{r}_j$, namely $r_{ij} = \|\mathbf{r}_j - \mathbf{r}_i\|$. Two constraints are defined to impose the constant length of the unit vectors $\mathbf{v}_i$ and $\mathbf{v}_j$. Three orientation constraints between pairs of vectors are finally introduced by exploiting the dot product and three constant, scalar parameters ϕ_1, ϕ_2 and ϕ_3, as shown in Fig. 2.

$$\boldsymbol{\Phi}_{rbc} = \begin{bmatrix} (\mathbf{r}_j - \mathbf{r}_i)^T(\mathbf{r}_j - \mathbf{r}_i) - r_{ij}^2 \\ \mathbf{v}_j^T\mathbf{v}_j - 1 \\ \mathbf{v}_i^T\mathbf{v}_i - 1 \\ (\mathbf{r}_j - \mathbf{r}_i)^T\mathbf{v}_j - r_{ij}\cos(\phi_1) \\ (\mathbf{r}_j - \mathbf{r}_i)^T\mathbf{v}_i - r_{ij}\cos(\phi_2) \\ \mathbf{v}_j^T\mathbf{v}_i - \cos(\phi_3) \end{bmatrix} = \mathbf{0} \tag{14}$$

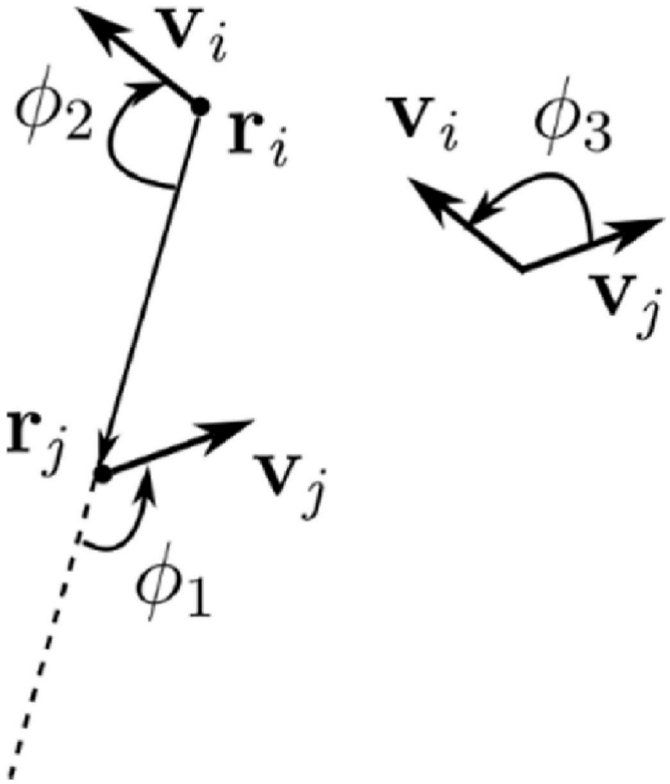

Fig. 2. NCs and angular parameters.

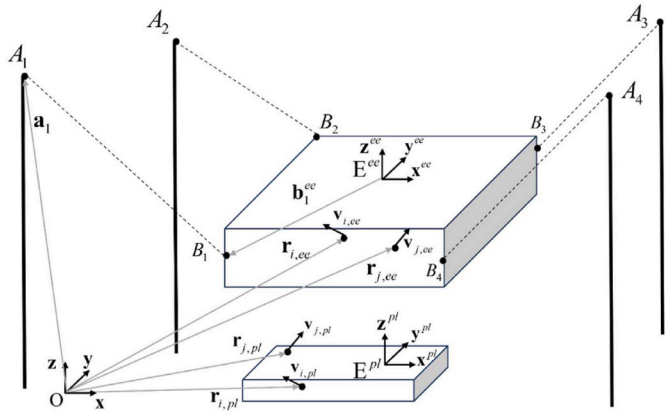

Fig. 3. EE of a CDPR and payload described through NCs.

3.3.3. External forces

An external lumped force $\mathbf{w}_e^f \in \mathbb{R}^3$ acting on a point $\mathbf{p}$ of the body (that is not a basic point of the NCs) is projected onto the NCs through matrix $\mathbf{C}_p^T$ ([17]):

$$\mathbf{f}_{ee} = \mathbf{C}_p^T \mathbf{w}_e^f, \tag{15}$$

where

$$\mathbf{C}_p = [\,(1-c_1)\mathbf{I}_{3\times3} \quad c_1\mathbf{I}_{3\times3} \quad c_2\mathbf{I}_{3\times3} \quad c_3\mathbf{I}_{3\times3}\,]. \tag{16}$$

c_k is the *k-th* element of vector $\mathbf{c}$ computed through $\mathbf{c} = \overline{\mathbf{X}}^{-1}(\overline{\mathbf{p}} - \overline{\mathbf{r}}_i)$ and $\overline{\mathbf{p}}$ is the counterpart of $\mathbf{p}$ expressed with respect to the local reference frame $\mathrm{E}_{\overline{xyz}}$.

When an external torque $\mathbf{w}_e^t \in \mathbb{R}^3$ is considered, it is firstly replaced by an equivalent pair of forces $\mathbf{w}_e^{f*}, -\mathbf{w}_e^{f*} \in \mathbb{R}^3$, with equal magnitudes (and opposite orientation), $\mathbf{w}_e^{f*} = (\mathbf{r}_j - \mathbf{r}_i) \times \mathbf{w}_e^t$, to be applied at the beginning and at the end of a unit vector $\mathbf{v}_{f*} = \frac{(\mathbf{r}_j - \mathbf{r}_i)\times\mathbf{w}_e^t}{\|(\mathbf{r}_j - \mathbf{r}_i)\times\mathbf{w}_e^t\|}$, which has $\mathbf{r}_i$ as origin.

The projection of these two forces is based on Eq. (15) through matrices $\mathbf{C}_{r_i}$ and $\mathbf{C}_{r_{f*}}$ (computed through Eq. (16) using $\mathbf{r}_{f*} = \mathbf{r}_i + \mathbf{v}_{f*}$), leading to the following term:

$$\mathbf{f}_{ee} = \left(\mathbf{C}_{r_i} - \mathbf{C}_{r_{f*}}\right)^T \mathbf{w}_e^{f*} \tag{17}$$

3.3.4. Application example: joining of two bodies

The use of DAEs together with the natural coordinates allows modelling an EE that picks an object (a payload), by creating a rigid connection between the two bodies The new dependent coordinates of the grasped body are added in vector of the dependent coordinates, while the same number of rigid body constraints are included among the kinematic constraints.

The two rotation matrices that describe the orientation of the two rigid bodies are $\mathbf{X}_{ee}$ (for the EE) and $\mathbf{X}_{pl}$ (for the payload), as defined in Eq. (7). The NCs describing the pose of the EE are gathered in vector $\mathbf{q}_{ee} \in \mathbb{R}^{12}$ and the mass matrix related to this subsystem is $\mathbf{M}_{ee} \in \mathbb{R}^{12\times12}$. The NCs describing the pose of the payload are collected in vector $\mathbf{q}_{pl} \in \mathbb{R}^{12}$, while $\mathbf{M}_{pl} \in \mathbb{R}^{12\times12}$ is its mass matrix. The whole vector of the dependent coordinates, by assuming a point-like representation of the cable EPs (see Section 4.1), is $\mathbf{q} = \left[\mathbf{q}_{ee}^T \quad \mathbf{q}_{pl}^T \quad \boldsymbol{\theta}^T\right]^T$, with $\boldsymbol{\theta} \in \mathbb{R}^{n_c}$ collecting the motor rotations. The resulting block-diagonal mass matrix $\mathbf{M}_m \in \mathbb{R}^{n_c\times n_c}$ is:

$$\mathbf{M} = \begin{bmatrix} \mathbf{M}_{ee} & \mathbf{0} & \mathbf{0} \\ \mathbf{0} & \mathbf{M}_{pl} & \mathbf{0} \\ \mathbf{0} & \mathbf{0} & \mathbf{M}_m \end{bmatrix} \tag{18}$$

The external forces are collected in vector $\mathbf{f} = \left[\mathbf{f}_{ee}^T \quad \mathbf{f}_{pl}^T \quad \boldsymbol{\tau}^T\right]^T$. The *i-th* cable enter in the robot workspace at point A_i and it is fixed to the EE at the *i-th* anchor point B_i. The payload is simulated to be in initial rest condition, and it is assumed that picking, i.e., the join between the two bodies, is performed with null relative speed. When the two objects are joined, the set of the constraint equations is enlarged to include the constraints representing the rigid connection $\boldsymbol{\Phi}_{rc} \in \mathbb{R}^6$. Such constraints are formed by three distance constraints $\boldsymbol{\Phi}_d \in \mathbb{R}^3$ and three orientation constraint $\boldsymbol{\Phi}_o \in \mathbb{R}^3$, and therefore constraint forces appears thanks to the Lagrange multipliers in Eq. (1). At the same time, the constraint force due to the frame, that counteracts gravity force, vanishes.

As shown in Fig. 4, the distance constraint relies on the definition of two points that describe the locations where the joining happens; such points are described through three Cartesian coordinates with respect to the local reference frame of the EE ($\mathrm{E}^{ee}_{\mathbf{x}^{ee}\mathbf{y}^{ee}\mathbf{z}^{ee}}$) $\mathbf{p}_1^{ee} \in \mathbb{R}^3$, and with respect

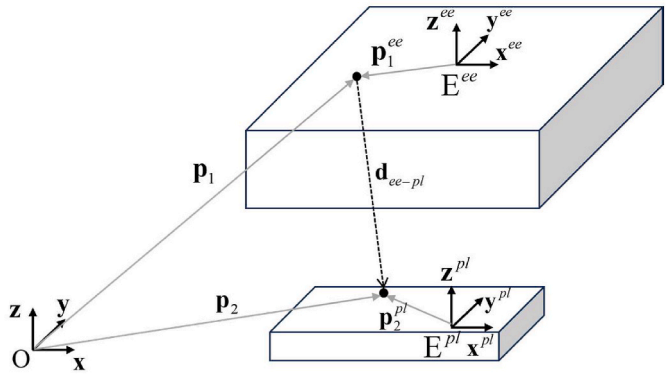

Fig. 4. Joining of two bodies.

to the local reference frame of the payload ($\mathrm{E}^{pl}_{\mathbf{x}^{pl}\mathbf{y}^{pl}\mathbf{z}^{pl}}$) $\mathbf{p}_2^{ee} \in \mathbb{R}^3$. The constant vector connecting the two points is $\mathbf{d}_{ee-pl} = \mathbf{p}_2 - \mathbf{p}_1 = \mathbf{C}_{p_2}\mathbf{q}_{pl} - \mathbf{C}_{p_1}\mathbf{q}_{ee}$. Once the rigid connection occurs, point $\mathbf{p}_2$ is enforced to be rigidly fixed to the EE, hence its Cartesian coordinates are $\mathbf{d}_{ee-pl} = \mathbf{C}_{d_{ee-pl}}\mathbf{q}_{ee}$. The components of $\mathbf{C}_{d_{ee-pl}}$ are computed through Eqs. (15) and (16) using $\mathbf{d}_{ee-pl}^{ee}$ and the rotation matrix $\mathbf{X}_{ee}$. As a result, the following distance constraint should be enforced:

$$\boldsymbol{\Phi}_d = \mathbf{C}_{p_2}\mathbf{q}_{pl} - \mathbf{C}_{p_1}\mathbf{q}_{ee} - \mathbf{C}_{d_{ee-pl}}\mathbf{q}_{ee} = \mathbf{0} \tag{19}$$

The remaining three constraints are the constant orientation constraints that rely on the definition of three angular parameters (χ_1, χ_2, χ_3), as shown in Fig. 5. The orientation constraints are reported in Eq. (20) and rely also on two vectors connecting two basic points of the EE ($\mathbf{l}_{ee} = \mathbf{r}_{j,ee} - \mathbf{r}_{i,ee}$) and of the payload ($\mathbf{l}_{pl} = \mathbf{r}_{j,pl} - \mathbf{r}_{i,pl}$), whose magnitudes are computed through $r_{ij,ee} = \|\mathbf{l}_{ee}\|$ and $r_{ij,pl} = \|\mathbf{l}_{pl}\|$:

$$\boldsymbol{\Phi}_o = \begin{bmatrix} \mathbf{l}_{ee}^T\mathbf{l}_{pl} - r_{ij,ee}r_{ij,pl}\cos(\chi_1) \\ \mathbf{v}_{j,ee}^T\mathbf{v}_{j,pl} - \cos(\chi_2) \\ \mathbf{v}_{i,ee}^T\mathbf{v}_{i,pl} - \cos(\chi_3) \end{bmatrix} = \mathbf{0} \tag{20}$$

The complete set of algebraic constraints therefore includes: the constraints related to the cables ($\boldsymbol{\Phi}_c$), the rigid body constraints for both the EE ($\boldsymbol{\Phi}_{rbc,ee}$) and the payload ($\boldsymbol{\Phi}_{rbc,pl}$) and the constraints representing the joining between the EE and the payload $\boldsymbol{\Phi}_{rc} = \left[\boldsymbol{\Phi}_d^T \quad \boldsymbol{\Phi}_o^T\right]^T$. Together, these set of constraints compose the full set $\boldsymbol{\Phi} =$

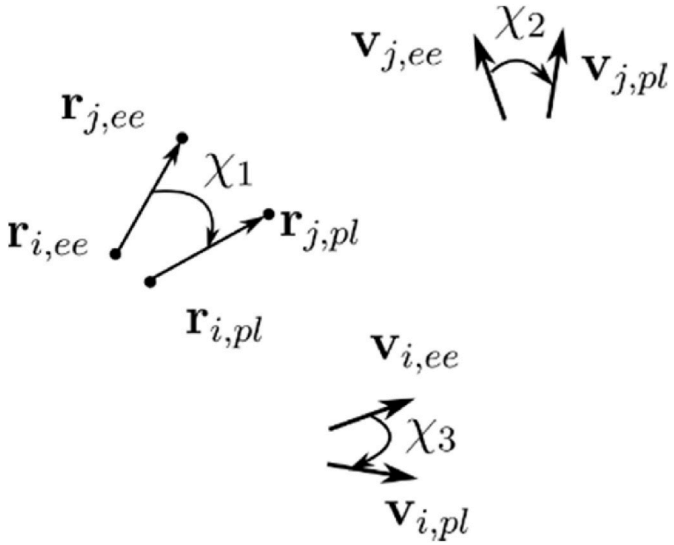

Fig. 5. Angular parameters.

$\left[\boldsymbol{\Phi}_c^T \quad \boldsymbol{\Phi}_{rbc,ee}^T \quad \boldsymbol{\Phi}_{rbc,pl}^T \quad \boldsymbol{\Phi}_{rc}^T\right]^T$ in Eq. (1).

3.3.5. Numerical example: joining of two bodies

The numerical test case proposed in this Section consists of three phases: an approaching stage of the EE that moves downward through a rest-to-rest vertical motion from the initial configuration to the "pick position". Then, the picking phase occurs. Finally, the CDPR lifts the payload through a vertical motion. The simulated CDPRs consists of an underactuated CDPR, with a 6-DOF EE actuated by four cables, to make visible the oscillations due to underactuation. The motors driving the four cables are controlled by four independent co-located PID controllers.

Both bodies are modelled as rectangular cuboids: the EE has a mass $m_{ee} = 62.8$ kg, while the payload has mass $m_{pl} = 6.28$ kg. By referring to Fig. 3, the two rigid bodies are modelled through NCs: those of the EE, $\mathbf{q}_{ee} = \left[\mathbf{r}_{i,ee}^T \quad \mathbf{r}_{j,ee}^T \quad \mathbf{v}_{i,ee}^T \quad \mathbf{v}_{j,ee}^T\right]^T$ and those of the payload $\mathbf{q}_{pl} = \left[\mathbf{r}_{i,pl}^T \quad \mathbf{r}_{j,pl}^T \quad \mathbf{v}_{i,pl}^T \quad \mathbf{v}_{j,pl}^T\right]^T$. Table 1 reports the initial values of the NCs, the absolute coordinates of vectors $\mathbf{a}_i$ that connect the origin of the global frame and the cable EPs A_i (that are assumed as fixed points B_i, as in Section 4.1), and the local coordinates of vectors $\mathbf{b}_i^{ee}$ connecting the anchor points with the local reference frame $\mathrm{E}^{ee}{}_{\mathbf{x}^{ee}\mathbf{y}^{ee}\mathbf{z}^{ee}}$ (see Fig. 3).

The origins of the body fixed reference frames $\mathrm{E}^{ee}{}_{\mathbf{x}^{ee}\mathbf{y}^{ee}\mathbf{z}^{ee}}$ and $\mathrm{E}^{pl}{}_{\mathbf{x}^{pl}\mathbf{y}^{pl}\mathbf{z}^{pl}}$ coincides respectively with the EE and payload CM. Moreover, the values of $\mathbf{r}_{i,ee}^{ee}$ and $\mathbf{r}_{i,pl}^{pl}$ are set to $\mathbf{r}_{i,ee}^{ee} = [0 \quad 0 \quad 0]^T$ m and $\mathbf{r}_{i,pl}^{pl} = [0 \quad 0 \quad 0]^T$ m. By referring to Fig. 4, the link connecting the two bodies, $\mathbf{d}_{ee-pl}$, starts from the CM of the EE ($\mathbf{p}_1{}^{ee} = [0 \quad 0 \quad 0]^T$ m) and reach the payload at location $\mathbf{p}_2{}^{pl} = [0.1 \quad 0.2 \quad 0]^T$ m.

The DAE-ODE conversion for solving the model has been done through the penalty formulation (see Refs. [3,16] for more details in its use for CDPRs), that exploits the following representation of the Lagrange multipliers, by means of three tuning parameters, α_p, ξ_p and ω_p:

$$\boldsymbol{\lambda} = \alpha_p\left(\ddot{\boldsymbol{\Phi}} + 2\xi_p\omega_p\dot{\boldsymbol{\Phi}} + \omega_p^2\boldsymbol{\Phi}\right) \tag{21}$$

In this test, by following a common rule-of-thumb in the literature, $\alpha_p = 10^8$, $\xi_p = 1$ and $\omega_p = 10^2$. By adopting a sample time $\Delta t = 1 \cdot 10^{-4}$ s (with a Runge-Kutta integration scheme), the simulation, lasting 20 s, just requires on average (over 10 simulations) 19.5 s. The model is solved in Matlab\Simulink running on a PC embedding an Intel Core i7-10700 CPU, by just exploiting one core.

The proposed model represents the step behaviour of gravity force, due to mass change at $t = 11$ s, and the related oscillating behaviour of tensions (see Fig. 6) and of the EE, represented in Fig. 7, through the Cartesian coordinates of the CM of the EE $\mathbf{r}_{i,ee} = \left[r_{i,ee}^x \quad r_{i,ee}^y \quad r_{i,ee}^z\right]^T$ and of the payload $\mathbf{r}_{i,pl} = \left[r_{i,pl}^x \quad r_{i,pl}^y \quad r_{i,pl}^z\right]^T$. Both figures clearly resemble a step response of an underactuated system, that oscillates with the system damped natural frequencies.

Table 1
Initial values of EE's NCs and payload's NCs, Cartesian coordinates of EPs and anchor points.

	EE		Payload
$\mathbf{r}_{i,ee}$ [m]	$[0\ 0\ 1.5]^T$	$\mathbf{r}_{i,pl}$ [m]	$[0\ 0\ 0]^T$
$\mathbf{r}_{j,ee}$ [m]	$[0\ 0.1\ 1.5]^T$	$\mathbf{r}_{j,pl}$ [m]	$[0\ 0.1\ 0]^T$
$\mathbf{v}_{i,ee}$ [–]	$[1\ 0\ 0]^T$	$\mathbf{v}_{i,pl}$ [–]	$[1\ 0\ 0]^T$
$\mathbf{v}_{j,ee}$ [–]	$[0\ 0\ 1]^T$	$\mathbf{v}_{j,pl}$ [–]	$[0\ 0\ 1]^T$
	EPs		Anchor points
$\mathbf{a}_1$ [m]	$[-1\ -1\ 2]^T$	$\mathbf{b}_1^{ee}$ [m]	$[-0.1\ -0.1\ 0]^T$
$\mathbf{a}_2$ [m]	$[-1\ 1\ 2]^T$	$\mathbf{b}_2^{ee}$ [m]	$[-0.1\ 0.1\ 0]^T$
$\mathbf{a}_3$ [m]	$[1\ 1\ 2]^T$	$\mathbf{b}_3^{ee}$ [m]	$[0.1\ 0.1\ 0]^T$
$\mathbf{a}_4$ [m]	$[1\ -1\ 2]^T$	$\mathbf{b}_4^{ee}$ [m]	$[0.1\ -0.1\ 0]^T$

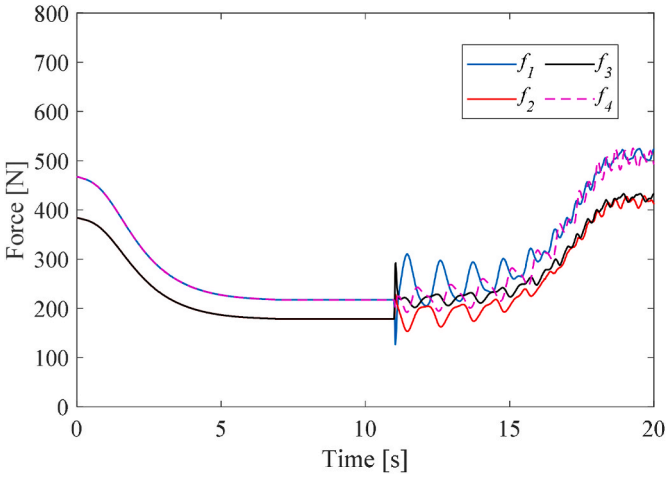

Fig. 6. Cable tensions behaviour during the simulation.

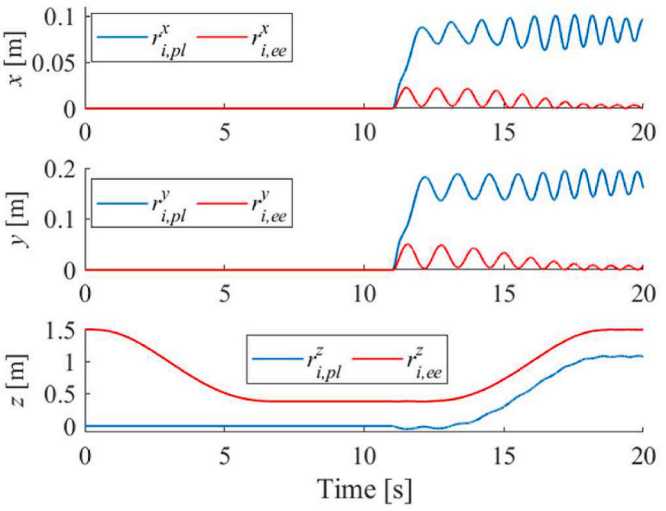

Fig. 7. Time-history of the EE and payload centres of mass.

4. Inclusion of the motors and guiding pulleys

The mass submatrix in in Eq. (1) related to the motor rotations θ_i is $\mathbf{M}_m = diag(J_{m,i})$, where $J_{m,i}$ denotes the moment of inertia of the *i-th* motor, $J_{m,i}$ (including the contributions of the rotor, the shaft, and the drum). The exerted torques are collected in $\mathbf{f}$ together with friction forces.

As for the guiding pulleys used to gather the cables in the robot workspace, there are different approaches to model them, depending on their features. In the following subsection the following modelling approaches are proposed.

- Point-like representation (Subsection 4.1)
- EPs with non-negligible dimensions and negligible moments of inertia (Subsection 4.2.1)
- EPs with non-negligible dimensions and moments of inertia (Subsection 4.2.2)

4.1. EPs: point-like representation

When guiding pulleys have negligible dimensions, if compared with the cable lengths, they can be simply modelled as points, typically are referred to as the "EPs". In such a case the global position of the A_i is described through the constant and known point $\mathbf{a}_i \in \mathbb{R}^3$ thus making the kinematic constraints in Eq. (2) directly employable within the set of DAEs without the need for other equations.

4.2. EPs: elements with non-negligible dimensions

Conversely, when the cable routing systems of a CDPR exploit guiding pulleys with non-negligible dimensions, the Cartesian coordinates of $\mathbf{a}_i$ change with the motion of the EE ([7]. [28–30]) Therefore, new coordinates should be included in the model and the algebraic constraint must be properly modified to account for their motion. In the following subsections, the kinematic relationships linking the *i-th* guiding pulley to the *i-th* anchor point on the EE is presented, by proposing both the ideal model of massless guiding pulleys (Section 4.2.1) and the case of pulleys with rotational inertia (Section 4.2.2).

4.2.1. Massless guiding pulleys

As a first simplified representation, the rotational moment of inertia about the swivel axis is neglected. This representation exploits 5 dependent coordinates for each cable ([7]), $(\boldsymbol{\delta}_i, \sigma_i, \mathbf{s}_i, \psi_i, \mathbf{n}_i)$ as explained in the following, without altering the number of DOFs. However, due to the assumption of negligible mass, the direct inclusion of $\boldsymbol{\delta}_i, \sigma_i, \mathbf{s}_i, \psi_i, \mathbf{n}_i$ within the set of redundant coordinates (together with 5 kinematic constraints) would lead to a singular mass matrix. Although this occurrence can be handled, e.g. through the penalty formulation, in this paper it is proposed a different approach to simplify the numerical solution of the equations of motion. The proposed approach does not increase the size of both $\mathbf{q}$ and $\boldsymbol{\Phi}$. In contrast, it treats $\boldsymbol{\delta}_i, \sigma_i, \mathbf{s}_i, \psi_i, \mathbf{n}_i$ as "intermediate" variables by means of the explicit formulation of the geometric dependencies between them and $\mathbf{q}$.

The geometry of the *i-th* guiding pulley is described by its radius $\widetilde{r}$. The *i-th* swivel pulley is associated to a local reference frame $(\mathbf{x}_i, \mathbf{y}_i, \mathbf{z}_i)$ that can be conveniently directed as the global axes of O_{xyz}. and has as origin point D_i. The spatial position of D_i is described through three Cartesian coordinates gathered in $\mathbf{d}_i \in \mathbb{R}^3$. The swivel axis of the pulley coincides to $\mathbf{z}_i$, which is tangent to the outer circumference. All these relevant quantities for the modelling of the swivel pulley are shown in Fig. 8.

The pulley lies on a plane which contains vector $\boldsymbol{\delta}_i = \mathbf{b}_i - \mathbf{d}_i$ and forms the angle σ_i, hereafter denoted as "swivel angle", with respect to the $\mathbf{z}_i\mathbf{x}_i$ plane. Such an angle can be easily retrieved through $\sigma_i = \text{atan } 2(\mathbf{y}_i \cdot \boldsymbol{\delta}_i, \mathbf{x}_i \cdot \boldsymbol{\delta}_i)$.

Two unit vectors, $\mathbf{s}_i$ and $\mathbf{n}_i$, must be introduced to compute the Cartesian coordinates of the EPs $\mathbf{a}_i$ where the cable leave the guiding pulley. $\mathbf{s}_i$ is the unit vector starting from $\mathbf{d}_i$ and heading to the center of the pulley (C_i); it is computed through $\mathbf{s}_i = \cos(\sigma_i)\mathbf{x}_i + \sin(\sigma_i)\mathbf{y}_i$. The angle ($\psi_i$) between $\mathbf{s}_i$ and $\mathbf{n}_i$ can be retrieved from Eq. (22) and it is exploited to assess the cable wrapping arc $\mathbf{d}_i\mathbf{a}_i$ which has a length $\|\mathbf{d}_i\mathbf{a}_i\| = \widetilde{r}(\pi - \psi_i)$.

$$\psi_i = 2\tan^{-1}\left(\frac{\boldsymbol{\delta}_i\cdot\mathbf{z}_i}{\boldsymbol{\delta}_i\cdot\mathbf{s}_i} + \sqrt{\left(\frac{\boldsymbol{\delta}_i\cdot\mathbf{z}_i}{\boldsymbol{\delta}_i\cdot\mathbf{s}_i}\right)^2 + 1 - \frac{2\widetilde{r}}{\boldsymbol{\delta}_i\cdot\mathbf{s}_i}}\right) \tag{22}$$

Finally, unit vector $\mathbf{n}_i$ is computed through $\mathbf{n}_i = \cos(\psi_i)\mathbf{s}_i + \sin(\psi_i)\mathbf{z}_i$ and, thus, $\mathbf{a}_i$ is retrieved from $\mathbf{a}_i = \mathbf{d}_i + \widetilde{r}(\mathbf{s}_i + \mathbf{n}_i)$. Therefore, the new algebraic constraint replacing Eq. (2) is:

$$\Phi_{c,i} = (\mathbf{b}_i - \mathbf{a}_i)\cdot(\mathbf{b}_i - \mathbf{a}_i) + \widetilde{r}^2(\pi - \psi_i)^2 + 2\widetilde{r}(\pi - \psi_i)\sqrt{(\mathbf{b}_i - \mathbf{a}_i)\cdot(\mathbf{b}_i - \mathbf{a}_i)} - r^2\theta_i^2 = 0 \tag{23}$$

that exploits the following intermediate algebraic calculations:

$$\begin{aligned}
&\boldsymbol{\delta}_i = \mathbf{b}_i - \mathbf{d}_i \\
&\sigma_i = \text{atan } 2(\mathbf{y}_i\cdot\boldsymbol{\delta}_i, \mathbf{x}_i\cdot\boldsymbol{\delta}_i) \\
&\mathbf{s}_i = \cos(\sigma_i)\mathbf{x}_i + \sin(\sigma_i)\mathbf{y}_i \\
&\tan(\psi_i/2) = \frac{\boldsymbol{\delta}_i\cdot\mathbf{z}_i}{\boldsymbol{\delta}_i\cdot\mathbf{s}_i} + \sqrt{\left(\frac{\boldsymbol{\delta}_i\cdot\mathbf{z}_i}{\boldsymbol{\delta}_i\cdot\mathbf{s}_i}\right)^2 + 1 - \frac{2\widetilde{r}}{\boldsymbol{\delta}_i\cdot\mathbf{s}_i}} \\
&\mathbf{n}_i = \cos(\psi_i)\mathbf{s}_i + \sin(\psi_i)\mathbf{z}_i
\end{aligned} \tag{24}$$

The partial derivative of Eq. (23), $\boldsymbol{\Phi}_{c,i/\mathbf{q}}$, and its time-derivative $\dot{\boldsymbol{\Phi}}_{c,i/\mathbf{q}}$ are detailed in appendix B.1.

4.2.2. Guiding pulleys with rotational inertia

When both radii and rotational moments of inertia of guiding pulleys are non-negligible, swivel angles must be treated as independent coordinates σ_i. One additional independent coordinate for each of the n_c cables is added thus leading to $\mathbf{q} = \begin{bmatrix}\mathbf{q}_{ee}^T & \boldsymbol{\sigma}^T & \boldsymbol{\theta}^T\end{bmatrix}^T \in \mathbb{R}^{12+2n_c}$ (to recall: 12 coordinates are adopted to represent the EE through NCs; n_c coordinates represent the motor rotations; n_c swivel angles are newly introduced). No additional constraints are defined within $\boldsymbol{\Phi}$. As in the model proposed in previous section, the other variables needed to represent the guiding pulleys (i.e., $\boldsymbol{\delta}_i, \mathbf{s}_i, \psi_i, \mathbf{n}_i$) are not included in $\mathbf{q}$ as dependent coordinates, to avoid mass matrix singularity. These four coordinates are treated, again, as "intermediate" variables by means of the explicit formulation of the geometric dependencies between them and $\mathbf{q}$. As far as the kinematic relations is concerned, Eq. (31) and Eq. (24) are still considered.

Therefore, by considering the swivel angles as generalized coordinates, the system has gained n_c DOFs since no new algebraic

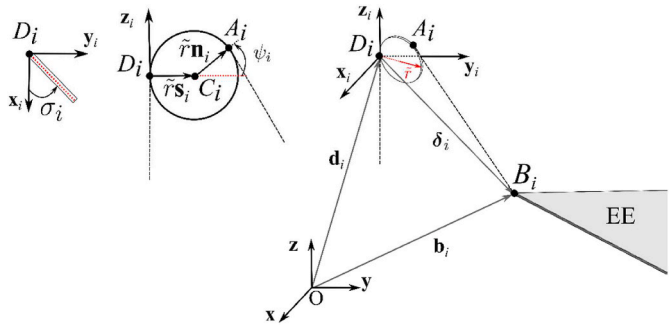

Fig. 8. Relevant parameters of the formulation.

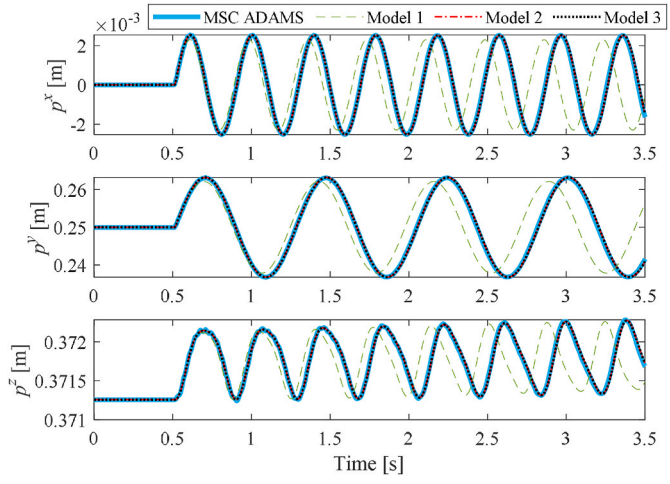

Fig. 9. Time-history of the CM of the ee.

constraints are introduced. Additionally, since n_c coordinates have been included, the model matrix size should consistently increase as well. In particular, $\mathbf{M}$ should include the diagonal submatrix with the rotational moments of inertia of guiding pulleys, J_{pulley_i}. The partial derivatives of Eq. (23) are reported in appendix B.2.

4.3. Numerical comparison

This Section provides a comparison between the three different models proposed in this section, by also comparing the results with those sported by MSC ADAMS (Figs. 9 and 10). The numerical test case consists of an underactuated CDPR with a 6-DOF EE driven by four motors, which makes it underactuated. The models proposed in this paper have been implemented in MatLab\Simulink. The EE has been modelled through redundant natural coordinates, as described in Section 3.3. The DAE to ODE conversion has been performed through the Udwadia-Kalaba method with the Baumgarte stabilization [16] (with both its tuning parameters equal to 10^3). The resulting ODEs have been integrated through the Runge-Kutta method, with a sampling time equal to $\Delta t = 1{\cdot}10^{-4}$ s.

The EE is a rectangular rigid body whose overall dimensions are $0.2\times 0.4\times 0.01$ m (along the x, y and z directions, respectively) and has a mass $m_{ee} = 6.24$ kg. The coordinates of the CM of the EE are gathered into $\mathbf{p} = [p^x \quad p^y \quad p^z]^T$ (whose initial value is $[0 \quad -0.25 \quad 0.37]^T$ m). The local reference frame $\mathrm{E}_{\overline{\mathbf{xyz}}}$ has no relative rotation with respect to the global reference frame. Table 2 reports the local $(\bar{\cdot})$ and the global Cartesian coordinates of points B_i and D_i.

The three formulations introduced in Section 5.1, 5.2.1 and 5.2.2 have been exploited to obtain three dynamic models of the CDPR (Model 1, 2 and 3 respectively).

Model 1 assumes that the cables enter in the robot workspace through known and fixed positions equal to the D_i points. In contrast, Model 2 and 3 account for the swivel pulleys radii that ($\bar{r} = 0.05$ m for all the pulleys). Model 2 dynamic model treats the swivel angles as dependent variables that are algebraically computed through Eq. (24). Model 3 represents the rotational inertias of the pulleys which have been set to $J_{pulley} = 5{\cdot}10^{-3}$ kgm^2 and includes swivel pulley rotations among the generalized (redundant) coordinates $\mathbf{q}^T = [\mathbf{q}_{ee}^T \quad \boldsymbol{\sigma}^T]^T$, with $\boldsymbol{\sigma} = [\sigma_1 \quad \sigma_2 \quad \sigma_3 \quad \sigma_4]^T$.

The EE is excited by an impulsive external force $\mathbf{f}_{ee} = [50 \quad 100 \quad 0]^T$ N applied at $\mathbf{p}$ from $t = 0.51$ s, to $t = 0.52$ s, that makes the load oscillating with its natural damped frequencies. During the simulation, the absolute displacement of $\mathbf{p}$ and the swivel angles $\boldsymbol{\sigma}$ have been tracked to compare the outcome different models, and the related computational efforts.

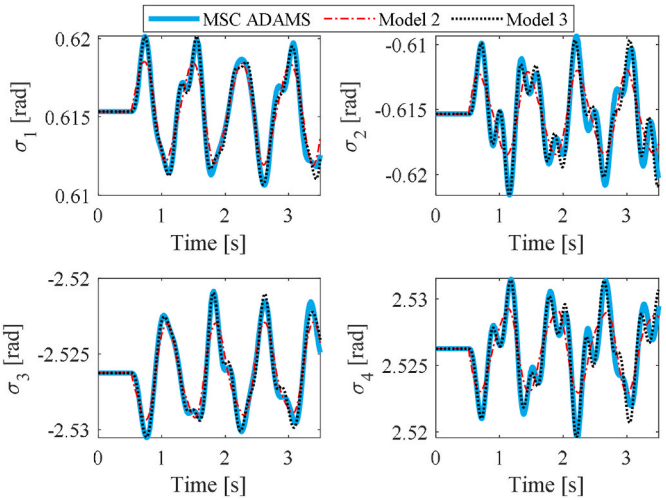

Fig. 10. Time-history of the swivel angles.

Table 2
Cartesian coordinates of B_i and D_i points.

$\bar{\mathbf{b}}_1$ [m]	$[-0.1 \quad -0.2 \quad 0]^T$	$\mathbf{d}_1$ [m]	$[-3.0 \quad -2.0 \quad 2.0]^T$
$\bar{\mathbf{b}}_2$ [m]	$[-0.1 \quad 0.2 \quad 0]^T$	$\mathbf{d}_2$ [m]	$[-3.0 \quad 2.5 \quad 2.0]^T$
$\bar{\mathbf{b}}_3$ [m]	$[0.1 \quad 0.2 \quad 0]^T$	$\mathbf{d}_3$ [m]	$[3.0 \quad 2.5 \quad 2.0]^T$
$\bar{\mathbf{b}}_4$ [m]	$[0.1 \quad -0.2 \quad 0]^T$	$\mathbf{d}_4$ [m]	$[3.0 \quad -2.0 \quad 2.0]^T$

It is noteworthy to highlight that MSC ADAMS exploits the "*cable system wizard*" to model cables, which requires defining the axial elasticity and the mass density of each cable. Additionally, the coupling between cables and pulleys imposes modelling the contact by means of static and dynamic frictions, the Hertzian contact forces and the penetration coefficients. All these features are not modelled in the proposed DAE-based model and are usually neglected in the literature. This model discrepancies leads to minimal differences among the model results. On the other hand, including the contact model remarkably increases the computational time to solve the model and introduces several uncertain parameters, whose values are difficult to evaluate in practical applications. Therefore, MSC ADAMS is here interpreted as a further comparative model instead of a benchmark to be exactly reproduced.

Fig. 9 and 10 show an excerpt of the overall simulation. No position drift has been experienced, thus proving that constraints are properly enforced. Fig. 9 shows the time-histories of the CM of the EE sported by all the simulators. Model 2, 3 and MSC ADAMS are almost overlapped, while Model 1 shows that neglecting the swivel pulley dimension leads to wrong estimation of the oscillation frequencies and amplitudes. A more detailed analysis is provided in Table 3 that summarizes the Root Mean Square (RMS) values of the differences with respect to the MSC ADAMS model (over the whole simulation lasting 10 s) and corroborates that MSC ADAMS and Model 2, 3 provide almost the same results with differences remarkably smaller than 1 mm. As for the differences in the estimated first damped natural frequency between Model 2, Model 3, and ADAMS, it is about the 0.5 %; this value is mainly related to the different friction models.

On the other hand, despite such negligible differences, the CPU time required by MSC ADAMS to simulate 10 s is 141.2 s (by averaging over 10 simulations), thus preventing its real-time implementation. In contrast, the numerical simulation of the proposed DAE-based models and performed through MatLab\Simulink is significantly smaller (although no code optimization has been performed to improve its computational effort and no parallel computing is exploited). The simulation of the three dynamic models requires 11.9 s, 9.1 s and 10.6 s, for Model 1, 2 and 3 respectively (by averaging over 10 simulations). Although real-time computation is still not achieved, it is reasonable supposing that code refinement, as well as parallel computing, might lead to real-time capability.

The four swivel angles, sported by MSC ADAMS and by the proposed Model 2 and 3, are shown in Fig. 10, by corroborating the similarity between the three models investigated. The RMS differences are summarized in Table 4.

5. Movable EPs

Another relevant feature that can be effectively modelled through DAEs is the presence of movable EPs, that leads to the so-called reconfigurable CDPRs ([20,21]). Two modelling approaches are proposed.

Table 3
RMS differences in EE's CM Cartesian coordinates.

	Model 1	Model 2	Model 3
$d_{p^x}^{RMS}$ [m]	$2.2{\cdot}10^{-3}$	$1.9{\cdot}10^{-4}$	$1.9{\cdot}10^{-4}$
$d_{p^y}^{RMS}$ [m]	$1{\cdot}10^{-2}$	$6.7{\cdot}10^{-4}$	$6.9{\cdot}10^{-4}$
$d_{p^z}^{RMS}$ [m]	$3.9{\cdot}10^{-4}$	$4.7{\cdot}10^{-5}$	$4.4{\cdot}10^{-5}$

Table 4
RMS differences on swivel angles.

	Model 2	Model 3
$d_{\sigma_1}^{RMS}$ [rad]	$7.1{\cdot}10^{-4}$	$6.9{\cdot}10^{-4}$
$d_{\sigma_2}^{RMS}$ [rad]	$1.5{\cdot}10^{-3}$	$1.7{\cdot}10^{-3}$
$d_{\sigma_3}^{RMS}$ [rad]	$7.1{\cdot}10^{-4}$	$6.7{\cdot}10^{-4}$
$d_{\sigma_4}^{RMS}$ [rad]	$1.5{\cdot}10^{-3}$	$1.6{\cdot}10^{-3}$

5.1. Full model approach

The full model approach includes the coordinates of the EPs ($\mathbf{q}_{a_i}$, with $i = 1, \ldots, n_{ep}$) among the independent coordinates. Therefore, the DAEs governing the system should be augmented with those representing the dynamics of such points. Such an approach is useful to study the whole system made by the robot and the movable EPs. On the other hand, it requires a precise dynamic model of such movable EPs (also including all the external forces acting on them, such as friction), that can be cumbersome to develop in some cases (e.g., in the case of an EP moved by a robot), and often are not of interest for the study of the CDPR.

5.2. Rheonomous constraints

As an alternative approach, the motion of the movable EPs is treated as rheonomous constraints. In practice it is assumed that the motion of the movable EPs is just a function of time ($\mathbf{a}_i(t)$, $\dot{\mathbf{a}}_i(t)$ and $\ddot{\mathbf{a}}_i(t)$), and is not affected by the motion of the CDPR coordinates. This assumption is reasonable in the presence of small inertia ratio or in the presence of effective controllers driving such EPs.

Rheonomous constraints are represented through the following position and time dependent kinematic constraint equations ([17]):

$$\begin{aligned} \boldsymbol{\Phi}(\mathbf{q},t) &= \mathbf{0} \\ \dot{\boldsymbol{\Phi}}(\mathbf{q},t) &= \boldsymbol{\Phi}_{/\mathbf{q}}\dot{\mathbf{q}} + \boldsymbol{\Phi}_{/t} = \mathbf{0} \\ \ddot{\boldsymbol{\Phi}}(\mathbf{q},t) &= \dot{\boldsymbol{\Phi}}_{/\mathbf{q}}\dot{\mathbf{q}} + \boldsymbol{\Phi}_{/\mathbf{q}}\ddot{\mathbf{q}} + \dot{\boldsymbol{\Phi}}_{/t} = \mathbf{0} \end{aligned} \tag{25}$$

In Eq. (25), the time-derivative of the rheonomous part of $\boldsymbol{\Phi}$ are introduced through $\boldsymbol{\Phi}_{/t}$ that is the partial derivative of the constraint equations with respect of time, and $\dot{\boldsymbol{\Phi}}_{/t} = d\boldsymbol{\Phi}_{/t}/dt$.

By exploiting the acceleration level of $\boldsymbol{\Phi}(\mathbf{q},t)$, the following index-1 DAEs can be obtained.

$$\begin{bmatrix} \mathbf{M} & \boldsymbol{\Phi}_{/\mathbf{q}}^T \\ \boldsymbol{\Phi}_{/\mathbf{q}} & \mathbf{0} \end{bmatrix} \begin{bmatrix} \ddot{\mathbf{q}} \\ \boldsymbol{\lambda} \end{bmatrix} = \begin{bmatrix} \mathbf{f} \\ -\dot{\boldsymbol{\Phi}}_{/\mathbf{q}}\dot{\mathbf{q}} - \dot{\boldsymbol{\Phi}}_{/t} \end{bmatrix} \tag{26}$$

It is evident how the rheonomous constraints affect the dynamics of the system by acting as external excitations. On the other hand, no information about the dynamic models of the EPs (and hence on the forces generating $\mathbf{a}_i(t)$) is required, thus remarkably simplify the model development and tuning.

5.3. Example: EE overturning in a CDPR with a reconfigurable EP

5.3.1. Test description

As stated in Section 3.3, the use of natural coordinates to represent the EE avoids pose singularities during numerical simulations. To provide evidence, the overturning of the EE of an underactuated reconfigurable CDPR has been numerically simulated. A rigid-body EE is actuated by $n_m = 2$ motors (and by n_m cables) and $n_{ep} = 1$ movable EPs has been considered.

The EE has been modelled through the NCs formulation presented in Section 3.3 and the NCs describing its pose have been collected in vector $\mathbf{q}_{ee} \in \mathbb{R}^{12}$ (the mass matrix of the EE is $\mathbf{M}_{ee} \in \mathbb{R}^{12\times12}$). The motor-driven cables are coiled around winches whose angular displacements are collected in vector $\boldsymbol{\theta} \in \mathbb{R}^{n_m}$; (the equivalent rotational inertias of the motors and winches are collected in the block-diagonal matrix $\mathbf{M}_m \in \mathbb{R}^{n_m\times n_m}$). Therefore, the vector of the generalized coordinates is $\mathbf{q} = \begin{bmatrix} \mathbf{q}_{ee}^T & \boldsymbol{\theta}^T \end{bmatrix}^T$, and the mass matrix of the CDPR is:

$$\mathbf{M} = \begin{bmatrix} \mathbf{M}_{ee} & \mathbf{0} \\ \mathbf{0} & \mathbf{M}_m \end{bmatrix} \tag{27}$$

The force vector collects the external forces acting on the EE ($\mathbf{f}_{ee}$) and the commanded torques ($\boldsymbol{\tau}$), namely $\mathbf{f} = \begin{bmatrix} \mathbf{f}_{ee}^T & \boldsymbol{\tau}^T \end{bmatrix}^T$. The full set of algebraic constraints of the dynamic model includes the 6 of rigid body constraints (see Eq. (14)), the n_m scleronomous, holonomic constraints related to the n_m cables with fixed EPs, and the n_{ep} rheonomous, holonomic constraints related to the reconfigurable EPs (by adopting the formulation of Section 6.2).

The reconfigurable EP is $\mathbf{a}_3(t)$; for the sake of simplicity, and without any lack of generality, its cable is assumed to have the fixed length $l_3 = 0.6$ m. The EE is modelled as a rigid body with a triangular shape and a mass $m_{ee} = 2.1$ kg. Table 5 collects the initial values of the NCs describing the EE pose ($\mathbf{q}_{ee} = \begin{bmatrix} \mathbf{r}_{i,ee}^T & \mathbf{r}_{j,ee}^T & \mathbf{v}_{i,ee}^T & \mathbf{v}_{j,ee}^T \end{bmatrix}^T$), the local Cartesian coordinates of the anchor points, collected in $\bar{\mathbf{b}}_i$ ($i = 1,2,3$), and the absolute Cartesian coordinates of the fixed EPs, collected in $\mathbf{a}_1$ and $\mathbf{a}_2$.

The motors have equal equivalent rotational inertias $J_m = 8.5{\cdot}10^{-5}$ kgm^2 and radii $r = 0.03$ m. The dynamic model has been obtained by employing the penalty formulation of Section 2.3.1 with the following parameter values $\alpha_p = 10^8$, $\xi_p = 1$ and $\omega_p = 10^2$. By adopting a simulation step size of $\Delta t = 1{\cdot}10^{-4}$ s the model is solved using the Runge-Kutta integration scheme. The numerical solution of the forward dynamics simulation lasting 14 s just requires 2.56 s (averaged over 10 runs).

The reconfigurable CDPR operates in open-loop control: the motors driving the cable lengths are commanded by means of pre-computed profiles; the reconfigurable EP is moved through 5th degree polynomial motion law from the initial $\mathbf{a}_3(t = 0)$, to a final $\mathbf{a}_3(t = T)$ configuration (with $T = 10$ s being the EP motion duration); from $t = 10$ s to $t = 14$ s the EP is required to be at rest.

5.3.2. Numerical results

Just some plots are shown here, to focus on the absence of singularities. Fig. 11 shows three sample captures of the simulation. The movable EP is represented through three coloured points, and the same colours are adopted to represent the EE: the red point represents the initial configuration, at $t = 0$ s; the green one represents an intermediate configuration just after overturning, at $t = 7.8$ s; the blue point represents the final configuration, at $t = 14$ s. The two fixed EP are represented through grey points.

Fig. 12 reports the "Z-Y-X" Euler angles (α, β and γ). Such angles have been retrieved from matrix $\mathbf{X}$, introduced in Eq. (7). It is evident that using the traditional minimal coordinate representation of the EE does not allow the overturning to be simulated since singularities are experienced at $t = 7.6$ s, thus corroborating the effectiveness of the NCs formulation exploited for the EE dynamic modelling.

Table 5
Initial values of EE's NCs, Cartesian coordinates of EPs and anchor points.

	NCs		EPs		Anchor points
$\mathbf{r}_{i,ee}$ [m]	$[0.4\ 1\ 0.6]^T$	$\mathbf{a}_1$ [m]	$[0\ 0\ 2]^T$	$\bar{\mathbf{b}}_1$ [m]	$[-0.09\ -0.15\ 0]^T$
$\mathbf{r}_{j,ee}$ [m]	$[0.5\ 1\ 0.6]^T$	$\mathbf{a}_2$ [m]	$[0\ 2\ 2]^T$	$\bar{\mathbf{b}}_2$ [m]	$[-0.09\ 0.15\ 0]^T$
$\mathbf{v}_{i,ee}$ [–]	$[0\ 1\ 0]^T$	$\mathbf{a}_3(t = 0)$ [m]	$[0.82\ 1\ 1.15]^T$	$\bar{\mathbf{b}}_3$ [m]	$[0.17\ 0\ 0]^T$
$\mathbf{v}_{j,ee}$ [–]	$[0\ 0\ 1]^T$	$\mathbf{a}_3(t = T)$ [m]	$[-0.68\ 1\ 1.3]^T$		

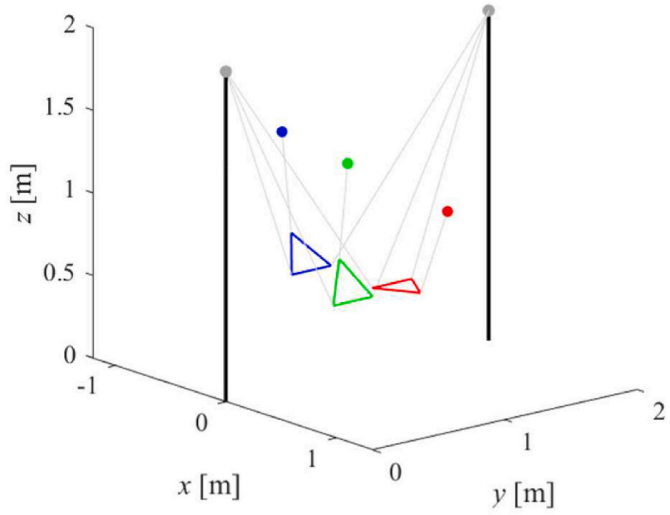

Fig. 11. Captures of the EE overturning.

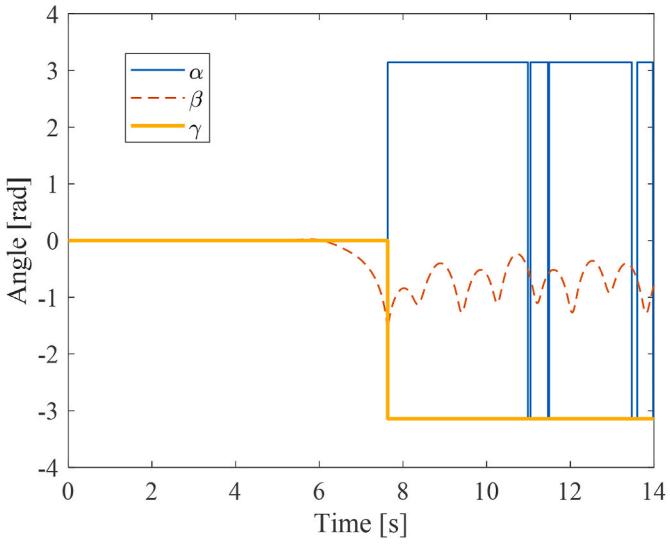

Fig. 12. "Z-Y-X" Euler angles during the overturning.

6. Conclusion

This paper proposes a comprehensive approach for modelling CDPRs. Whilst these robots are usually modelled in the literature through ODEs, this work uses a multibody system perspective and therefore exploits DAEs. Such an approach allows for the straightforward inclusion of several features of CDPRs, also including some non-ideal behaviours whose representation through ODEs is often very cumbersome, since DAEs deal with a set of redundant coordinates and embed algebraic kinematic constraints within the equations of motions. The following components of a CDPRs are discussed, by providing details on their model development and solution.

- 6-DOF end-effectors, whose representation through Natural Coordinates is proposed to avoid singularities and to easily represents object picking;
- rigid cables, that are modelled by exploiting the kinematic constraint equations and the Lagrange multipliers;
- redundant cables, that can be easily handled by converting the DAEs to redundant ODEs;
- driving motors, that are easily embedded in the model by exploiting the redundant coordinates, and hence augmenting the model coordinates with the motor rotations, thus avoiding cumbersome calculations to condensate them within the minimal coordinates;
- guiding pulleys with non-negligible dimensions, that can be either represented through dependent coordinates whenever moments of inertia of these components are negligible, or alternatively through some additional independent coordinates;
- movable robot EPs, as those often used in reconfigurable CDPRs, that are treated as rheonomous constraints, thus avoiding the dynamic modelling of the subsystem used to drive such points.

Some numerical tests, also comparing the results with those sported by MSC ADAMS, show the method correctness, its reduced computational effort and the easiness of formulation, that make it a good candidate for developing accurate simulators of CDPRs.

Conflict of interest

The authors declare that they have no known competing financial interests or personal relationships that could have influenced the work reported in this paper.

CRediT authorship contribution statement

Giulio Piva: Conceptualization, Data curation, Investigation, Methodology, Software, Validation, Writing – original draft. **Dario Richiedei:** Conceptualization, Formal analysis, Investigation, Methodology, Validation, Visualization, Writing – original draft, Writing – review & editing. **Alberto Trevisani:** Funding acquisition, Project administration, Resources, Supervision.

Declaration of competing interest

The authors declare the following financial interests/personal relationships which may be considered as potential competing interests: Alberto Trevisani reports financial support was provided by European Union Next-GenerationEU - consortium iNEST. Alberto Trevisani reports financial support was provided by Italian Ministry of University and Research. The authors declare that they have no known competing financial interests or personal relationships that could have influenced the work reported in this paper If there are other authors, they declare that they have no known competing financial interests or personal relationships that could have appeared to influence the work reported in this paper.

Data availability

Data will be made available on request.

Acknowledgement

This work is part of the Co-MIR PRIN-2020 project (Prot.2020C-MEFPK) funded by the Italian Ministry of University and Research. This study was also developed within the PNRR research activities of the consortium iNEST (Interconnected North-Est Innovation Ecosystem) funded by the European Union Next-GenerationEU (Piano Nazionale di Ripresa e Resilienza (PNRR) – Missione 4 Componente 2, Investimento 1.5 – D.D. 1058 June 23, 2022, ECS_00000043). This manuscript reflects only the Authors' views and opinions, neither the European Union nor the European Commission can be considered responsible for them.

Appendix A

A. Cable tension computation

The reaction forces introduced by the kinematic constraints, $\mathbf{f}_c \in \mathbb{R}^{n_q}$, are represented through the term $\mathbf{\Phi}_{\mathbf{q}}^T \boldsymbol{\lambda} \in \mathbb{R}^{n_q}$. Among these forces, the contribution of cable tensions projected onto the direction of the model coordinates is therefore computed as follows

$$\mathbf{f}_c = \begin{bmatrix} \mathbf{\Phi}^T_{/\mathbf{q}_{nc}} \\ \vdots \end{bmatrix} \boldsymbol{\lambda} \tag{28}$$

where $\mathbf{\Phi}_{c/\mathbf{q}_{nc}} = \left[\frac{\partial \mathbf{\Phi}_c}{\partial \mathbf{q}_{nc}}\right]$ consider just the constraints related to cables.

Generally speaking, the *i-th* cable tension produces an effect on the EE coordinates equal to $\mathbf{f}_{cable,i} = \Phi^T_{c,i/\mathbf{q}_{nc}} \lambda_i$, where $\Phi_{c,i/\mathbf{q}_{nc}}$ is the partial derivative of the *i-th* cable constraint with respect to the set of NCs and the total effect of all cable forces can be evaluated through $\sum_{i=1}^{n_c} \mathbf{f}_{cable,i}$.

In addition, $\mathbf{f}_{cable,i} = \Phi^T_{c,i/\mathbf{q}_{nc}} \lambda_i$ can be usefully exploited to compute the magnitude and the direction of the cable tension, respectively, through $f_i = \left\| \mathbf{f}_{cable,i} \right\|$ and $\mathbf{u}_i = -\frac{\mathbf{C}_{b_i} \Phi^T_{c,i/\mathbf{q}_{nc}}}{\left\| \mathbf{C}_{b_i} \Phi^T_{c,i/\mathbf{q}_{nc}} \right\|}$.

B. Analytical derivation of constraint Jacobian matrix for inclusion of guiding pulleys

B.1 Without rotational inertia

This subsection provides the analytical derivation of the time-derivative of Eq. (23) for the case of massless guiding pulleys with non-negligible geometry (see Section 4.2.1). The assumption of modelling the EE through NCs ($\mathbf{q}_{ee} \in \mathbb{R}^{12}$) is made, therefore the Cartesian coordinates of the *i-th* anchor point are retrieved through $\mathbf{b}_i = \mathbf{C}_{b_i} \mathbf{q}_{ee}$.

The constraint Jacobian matrix for the algebraic constraints of Eq. (23) takes the form:

$$\mathbf{\Phi}_{c/\mathbf{q}} = \begin{bmatrix} \mathbf{\Phi}_{c/\mathbf{q}_{ee}} & \mathbf{\Phi}_{c/\boldsymbol{\theta}} \end{bmatrix} \tag{29}$$

By referring to Eq (29), the analytical form of the two submatrices, $\mathbf{\Phi}_{c/\mathbf{q}_{ee}}$ and $\mathbf{\Phi}_{c/\boldsymbol{\theta}}$ is here reported. The *i-th* row of submatrix $\mathbf{\Phi}_{c/\mathbf{q}_{ee}}$ is computed by substituting $\mathbf{b}_i = \mathbf{C}_{b_i} \mathbf{q}_{ee}$ in Eq. (23) and differentiating it with respect to $\mathbf{q}_{ee}$:

$$\Phi_{c,i/\mathbf{q}_{ee}} = 2\left(1 + \frac{\widetilde{r}(\pi - \psi_i)}{\sqrt{\boldsymbol{\mu}_i \cdot \boldsymbol{\mu}_i}}\right)\left(\mathbf{C}_{b_i} \mathbf{q}_{ee} - \mathbf{a}_i\right)^T \mathbf{C}_{b_i} \tag{30}$$

which can be rewritten in compact form as

$$\Phi_{c,i/\mathbf{q}_{ee}} = \widetilde{f}\,\widetilde{g} \tag{31}$$

where the terms $\widetilde{f}$ and $\widetilde{g}$ are

$$\widetilde{f} = 2\left(1 + \frac{\widetilde{r}(\pi - \psi_i)}{\sqrt{\boldsymbol{\mu}_i \cdot \boldsymbol{\mu}_i}}\right) \quad \widetilde{g} = \left(\mathbf{C}_{b_i} \mathbf{q}_{ee} - \mathbf{a}_i\right)^T \mathbf{C}_{b_i} \tag{32}$$

$\mathbf{\Phi}_{c/\boldsymbol{\theta}}$ submatrix is a diagonal matrix whose elements are $\Phi_{c,i/\theta_i} = -2r^2\theta_i$, with $i = 1, \ldots, n_m$.

Then, the time-derivative of Eq. (29) is:

$$\dot{\mathbf{\Phi}}_{c/\mathbf{q}} = \begin{bmatrix} \dot{\mathbf{\Phi}}_{c/\mathbf{q}_{ee}} & \dot{\mathbf{\Phi}}_{c/\boldsymbol{\theta}} \end{bmatrix} \tag{33}$$

and the analytical form of time-derivatives of its submatrices ($\mathbf{\Phi}_{c/\mathbf{q}_{ee}}$ and $\mathbf{\Phi}_{c/\boldsymbol{\theta}}$) is here reported. The elements of the $\dot{\mathbf{\Phi}}_{c/\boldsymbol{\theta}}$ diagonal submatrix can be straightforwardly computed as $\dot{\Phi}_{c,i/\theta_i} = -2r^2\dot{\theta}_i$, with $i = 1, \ldots, n_m$. Conversely, the terms encompassed in $\dot{\mathbf{\Phi}}_{c/\mathbf{q}_{ee}}$ require a more involved formulation. By taking the time-derivative of Eq. (31), one gets:

$$\dot{\Phi}_{c,i/\mathbf{q}_{ee}} = \frac{d}{dt}\left[\widetilde{f}\,\widetilde{g}\right] = \dot{\widetilde{f}}\,\widetilde{g} + \widetilde{f}\,\dot{\widetilde{g}} \tag{34}$$

Where time-derivatives of $\widetilde{f}$ and $\widetilde{g}$ are defined as follows.

$$\dot{\widetilde{f}} = -\frac{2\widetilde{r}\dot{\psi}_i\sqrt{\boldsymbol{\mu}_i \cdot \boldsymbol{\mu}_i} + \frac{2\widetilde{r}(\pi - \psi_i)\left(\mathbf{C}_{b_i}\dot{\mathbf{q}}_{ee} - \dot{\mathbf{a}}_i\right)\cdot\left(\mathbf{C}_{b_i}\mathbf{q}_{ee} - \mathbf{a}_i\right)}{\sqrt{\boldsymbol{\mu}_i \cdot \boldsymbol{\mu}_i}}}{\boldsymbol{\mu}_i \cdot \boldsymbol{\mu}_i} \quad \dot{\widetilde{g}} = \left(\mathbf{C}_{b_i}\dot{\mathbf{q}}_{ee} - \dot{\mathbf{a}}_i\right)^T \mathbf{C}_{b_i} \tag{35}$$

In order to compute Eq. (35), the analytical expression of the $\dot{\mathbf{a}}_i$, $\dot{\mathbf{n}}_i$, $\dot{\mathbf{s}}_i$, $\dot{\sigma}_i$ and $\dot{\psi}_i$ terms must be available. In the following, the analytical derivation of such terms is proposed.

By supposing that $\dot{\mathbf{d}}_i(t) = \mathbf{0}\ \forall t$, the time-derivative of $\mathbf{a}_i$, can be computed as follows.

$$\dot{\mathbf{a}}_i = \widetilde{r}(\dot{\mathbf{s}}_i + \dot{\mathbf{n}}_i) \tag{36}$$

Equation (36) requires the analytical expressions for $\dot{\mathbf{n}}_i$ and $\dot{\mathbf{s}}_i$, which are reported here below.

$$\begin{aligned}\dot{\mathbf{n}}_i &= \cos(\psi_i)\dot{\mathbf{s}}_i - \sin(\psi_i)\dot{\psi}_i\mathbf{s}_i + \cos(\psi_i)\dot{\psi}_i\mathbf{z}_i \\ \dot{\mathbf{s}}_i &= (-\sin(\sigma_i)\mathbf{x}_i + \cos(\sigma_i)\mathbf{y}_i)\dot{\sigma}_i\end{aligned} \tag{37}$$

In order to compute $\dot{\mathbf{s}}_i$ the expression of $\dot{\sigma}_i$ needs to be available, therefore, by recalling that $\sigma_i = \text{atan}\,2(\mathbf{y}_i\cdot\boldsymbol{\delta}_i, \mathbf{x}_i\cdot\boldsymbol{\delta}_i)$, $\dot{\sigma}_i$ can be computed as follows.

$$\dot{\sigma}_i = \frac{(\mathbf{x}_i\cdot\boldsymbol{\delta}_i)(\mathbf{y}_i\cdot\dot{\boldsymbol{\delta}}_i) - (\mathbf{x}_i\cdot\dot{\boldsymbol{\delta}}_i)(\mathbf{y}_i\cdot\boldsymbol{\delta}_i)}{(\mathbf{x}_i\cdot\boldsymbol{\delta}_i)^2 + (\mathbf{y}_i\cdot\boldsymbol{\delta}_i)^2} \tag{38}$$

The analytical expression of $\dot{\psi}_i$, which needs to be available to compute Eqs. (37)-(35), is reported here below. For sake of clarity, the analytical equation of angle $\psi_i = 2\tan^{-1}\left(\frac{\mathbf{z}_i\cdot\boldsymbol{\delta}_i}{\mathbf{s}_i\cdot\boldsymbol{\delta}_i} + \sqrt{\left(\frac{\mathbf{z}_i\cdot\boldsymbol{\delta}_i}{\mathbf{s}_i\cdot\boldsymbol{\delta}_i}\right)^2 + 1 - \frac{2\widetilde{r}}{\mathbf{s}_i\cdot\boldsymbol{\delta}_i}}\right)$ can be rewritten in compact form by introducing three terms, namely $\widetilde{\alpha} = \frac{\mathbf{z}_i\cdot\boldsymbol{\delta}_i}{\mathbf{s}_i\cdot\boldsymbol{\delta}_i}$, $\widetilde{\beta} = \frac{2\widetilde{r}}{\mathbf{s}_i\cdot\boldsymbol{\delta}_i}$ and $\eta = \widetilde{\alpha} + \sqrt{\widetilde{\alpha}^2 + 1 - \widetilde{\beta}}$.

$$\psi_i = 2\tan^{-1}\left(\widetilde{\alpha} + \sqrt{\widetilde{\alpha}^2 + 1 - \widetilde{\beta}}\right) = 2\tan^{-1}(\eta) \tag{39}$$

Therefore, the time-derivative of Eq. (39) takes the following form.

$$\dot{\psi}_i = \frac{2}{1+\eta^2}\dot{\eta} \tag{40}$$

Equation (40) requires the expressions of terms $\dot{\eta}$, $\dot{\widetilde{\beta}}$ and $\dot{\widetilde{\alpha}}$, which take the following forms.

$$\dot{\eta} = \dot{\widetilde{\alpha}} + \frac{2}{\sqrt{\widetilde{\alpha}^2 + 1 - \widetilde{\beta}}}(\widetilde{\alpha}\dot{\widetilde{\alpha}} - \dot{\widetilde{\beta}})\dot{\widetilde{\beta}} = -\frac{\widetilde{r}(\dot{\mathbf{s}}_i\cdot\boldsymbol{\delta}_i + \mathbf{s}_i\cdot\dot{\boldsymbol{\delta}}_i)}{(\mathbf{s}_i\cdot\boldsymbol{\delta}_i)^2}\dot{\widetilde{\alpha}} = \frac{(\mathbf{z}_i\cdot\dot{\boldsymbol{\delta}}_i)(\mathbf{s}_i\cdot\boldsymbol{\delta}_i) - (\mathbf{z}_i\cdot\boldsymbol{\delta}_i)(\dot{\mathbf{s}}_i\cdot\boldsymbol{\delta}_i + \mathbf{s}_i\cdot\dot{\boldsymbol{\delta}}_i)}{(\mathbf{s}_i\cdot\boldsymbol{\delta}_i)^2} \tag{41}$$

B.2 With rotational inertia

This subsection provides the analytical derivation of the time-derivative of Eq. (23) for the case of guiding pulleys with non-negligible geometry and moment of inertia (see Section 4.2.2). The assumption of modelling the EE $\mathbf{q}_{ee} \in \mathbb{R}^{12}$ through NCs is made, therefore the Cartesian coordinates of the *i-th* anchor point are retrieved through $\mathbf{b}_i = \mathbf{C}_{b_i}\mathbf{q}_{ee}$.

Since σ_i and $\dot{\sigma}_i$ belong to $\mathbf{q}$ and the constraint Jacobian matrix changes with respect to Eq. (29) and is structured as follows:

$$\boldsymbol{\Phi}_{c/\mathbf{q}} = \begin{bmatrix}\boldsymbol{\Phi}_{c/\mathbf{q}_{ee}} & \boldsymbol{\Phi}_{c/\boldsymbol{\sigma}} & \boldsymbol{\Phi}_{c/\boldsymbol{\theta}}\end{bmatrix} \tag{42}$$

the analytical expression of the diagonal submatrix $\boldsymbol{\Phi}_{c/\boldsymbol{\sigma}}$ can be retrieved by exploiting Eq (30). The expression for the *-th* element Φ_{c,σ_i} is reported here below.

$$\Phi_{c,\sigma_i} = 2\mathbf{a}_{i,\sigma_i}\cdot\boldsymbol{\mu}_i + 2\widetilde{r}^2\psi_{i,\sigma_i}(\psi_i - \pi) + 2\left(\frac{\widetilde{r}(\pi - \psi_i)\mathbf{a}_{i,\sigma_i}\cdot\boldsymbol{\mu}_i}{\sqrt{\boldsymbol{\mu}_i\cdot\boldsymbol{\mu}_i}} - \widetilde{r}\psi_{i,\sigma_i}\sqrt{\boldsymbol{\mu}_i\cdot\boldsymbol{\mu}_i}\right) \tag{43}$$

In order to compute Eq. (43), the analytical expressions of $\mathbf{a}_{i/\sigma_i}$, $\mathbf{n}_{i/\sigma_i}$, $\mathbf{s}_{i/\sigma_i}$, $\widetilde{\alpha}_{/\sigma_i}$, $\eta_{/\sigma_i}$, and ψ_{i/σ_i} need to be available. The analytical expression of term $\mathbf{a}_{i/\sigma_i}$ takes the following form.

$$\mathbf{a}_{i/\sigma_i} = \widetilde{r}(\mathbf{s}_{i/\sigma_i} + \mathbf{n}_{i/\sigma_i}) \tag{44}$$

Therefore, $\mathbf{s}_{i/\sigma_i}$ and $\mathbf{n}_{i/\sigma_i}$ must be computed as follows:

$$\begin{aligned}\mathbf{s}_{i/\sigma_i} &= \cos(\sigma_i)\mathbf{y}_i - \sin(\sigma_i)\mathbf{x}_i \\ \mathbf{n}_{i/\sigma_i} &= \cos(\psi_i)\mathbf{s}_{i/\sigma_i} - \sin(\psi_i)\psi_{i/\sigma_i}\mathbf{s}_i + \cos(\psi_i)\psi_{i/\sigma_i}\mathbf{z}_i\end{aligned} \tag{45}$$

It is evident that, in order to compute Eq. (45) the equation of ψ_{i/σ_i} should be available. By recalling Eq. (39), term ψ_{i/σ_i} takes the following expression

$$\psi_{i/\sigma_i} = \frac{2}{1+\eta^2}\eta_{/\sigma_i} \tag{46}$$

which requires the computation of $\eta_{/\sigma_i}$ and $\widetilde{\alpha}_{/\sigma_i}$.

$$\begin{aligned}\eta_{/\sigma_i} &= \widetilde{\alpha}_{/\sigma_i} + \frac{1}{\sqrt{\widetilde{\alpha}^2 + 1 - \widetilde{\beta}}}\left(\widetilde{\alpha}\widetilde{\alpha}_{/\sigma_i} + \widetilde{r}\frac{\boldsymbol{\delta}_i\cdot\mathbf{s}_{i/\sigma_i}}{(\mathbf{s}_i\cdot\boldsymbol{\delta}_i)^2}\right) \\ \widetilde{\alpha}_{/\sigma_i} &= -\frac{(\boldsymbol{\delta}_i\cdot\mathbf{s}_{i/\sigma_i})(\mathbf{z}_i\cdot\boldsymbol{\delta}_i)}{(\mathbf{z}_i\cdot\boldsymbol{\delta}_i)^2}\end{aligned} \tag{47}$$

The time-derivative of Eq. (42) is straightforwardly composed as:

$$\dot{\boldsymbol{\Phi}}_{c/\mathbf{q}} = \begin{bmatrix}\dot{\boldsymbol{\Phi}}_{c/\mathbf{q}_{ee}} & \dot{\boldsymbol{\Phi}}_{c/\boldsymbol{\sigma}} & \dot{\boldsymbol{\Phi}}_{c/\boldsymbol{\theta}}\end{bmatrix} \tag{48}$$

which involves the submatrices $\dot{\mathbf{\Phi}}_{c/\mathbf{q}_{ee}}$ and $\dot{\mathbf{\Phi}}_{c/\boldsymbol{\theta}}$, that have been derived in the previous Section, and diagonal submatrix $\dot{\mathbf{\Phi}}_{c/\boldsymbol{\sigma}}$ whose elements are the time-derivative of Eq. (43), namely $\dot{\Phi}_{c,i/\sigma_i}$. For sake of clarity, it is useful to decompose the analytical expression of $\dot{\Phi}_{c,i/\sigma_i}$ as the sum of three terms $\dot{\Phi}_{c,i/\sigma_i} = \dot{\Phi}^{\mathrm{I}}_{c,i/\sigma_i} + \dot{\Phi}^{\mathrm{II}}_{c,i/\sigma_i} + \dot{\Phi}^{\mathrm{III}}_{c,i/\sigma_i}$. Such terms take the following analytical expressions.

$$\begin{aligned}
\dot{\Phi}^{\mathrm{I}}_{c,\frac{i}{\sigma_i}} &= 2\left(\dot{\mathbf{a}}_{i/\sigma_i}\cdot\boldsymbol{\mu}_i + \left(\dot{\mathbf{a}}_i\text{-}\mathbf{C}_{b_i}\dot{\mathbf{q}}_{ee}\right)\cdot\mathbf{a}_{i/\sigma_i}\text{-}\tilde{r}\dot{\psi}_{i/\sigma_i}\frac{\left(\mathbf{C}_{b_i}\dot{\mathbf{q}}_{ee}\text{-}\dot{\mathbf{a}}_i\right)\cdot\left(\mathbf{C}_{b_i}\mathbf{q}_{ee}\text{-}\mathbf{a}_i\right)}{\sqrt{\boldsymbol{\mu}_i\cdot\boldsymbol{\mu}_i}}\tilde{r}\dot{\psi}_{i/\sigma_i}\sqrt{\boldsymbol{\mu}_i\cdot\boldsymbol{\mu}_i}\right)\\
\dot{\Phi}^{\mathrm{II}}_{c,\frac{i}{\sigma_i}} &= -2\left(\tilde{r}\dot{\psi}_{i/\sigma_i}\frac{\boldsymbol{\mu}_i\cdot\mathbf{a}_{i/\sigma_i}}{\sqrt{\boldsymbol{\mu}_i\cdot\boldsymbol{\mu}_i}} + \tilde{r}(\pi\text{-}\psi_i)\frac{\left(\mathbf{C}_{b_i}\dot{\mathbf{q}}_{ee}\text{-}\dot{\mathbf{a}}_i\right)\cdot\left(\mathbf{C}_{b_i}\mathbf{q}_{ee}\text{-}\mathbf{a}_i\right)}{\left(\boldsymbol{\mu}_i\cdot\boldsymbol{\mu}\right)^{3/2}}\mathbf{a}_{i/\sigma_i}\cdot\boldsymbol{\mu}_i\right)\\
\dot{\Phi}^{\mathrm{III}}_{c,\frac{i}{\sigma_i}} &= 2\tilde{r}(\pi\text{-}\psi_i)\left(\frac{\left(\dot{\mathbf{a}}_i\text{-}\mathbf{C}_{b_i}\dot{\mathbf{q}}_{ee}\right)\cdot\mathbf{a}_{i/\sigma_i}\text{-}\boldsymbol{\mu}_i\cdot\dot{\mathbf{a}}_{i/\sigma_i}}{\sqrt{\boldsymbol{\mu}_i\cdot\boldsymbol{\mu}_i}}\right.
\end{aligned} \tag{49}$$

In order to compute the terms of Eq. (49), it is necessary the availability of the expressions of $\dot{\mathbf{a}}_{i/\sigma_i}$, $\dot{\mathbf{n}}_{i/\sigma_i}$, $\dot{\mathbf{s}}_{i/\sigma_i}$, $\dot{\psi}_{i/\sigma_i}$, $\dot{\eta}_{/\sigma_i}$, $\dot{\tilde{\alpha}}_{/\sigma_i}$, and $\dot{\tilde{\beta}}_{/\sigma_i}$ terms. The time-derivative of $\mathbf{a}_{i/\sigma_i}$ is basically:

$$\dot{\mathbf{a}}_{i/\sigma_i} = \tilde{r}\left(\dot{\mathbf{s}}_{i/\sigma_i} + \dot{\mathbf{n}}_{i/\sigma_i}\right) \tag{50}$$

where $\dot{\mathbf{s}}_{i/\sigma_i}$ and $\dot{\mathbf{n}}_{i/\sigma_i}$ can be computed as follows.

$$\begin{aligned}
\dot{\mathbf{s}}_{i/\sigma_i} &= -\dot{\sigma}_i\cos(\sigma_i)\mathbf{x}_i - \dot{\sigma}_i\sin(\sigma_i)\mathbf{y}_i\\
\dot{\mathbf{n}}_{i/\sigma_i} &= -\sin(\psi_i)\dot{\psi}_{i/\sigma_i}\mathbf{s}_i - \sin(\psi_i)\psi_{i/\sigma_i}\dot{\mathbf{s}}_i - \dot{\psi}_i\cos(\psi_i)\psi_{i/\sigma_i}\mathbf{s}_i - \dot{\psi}_i\sin(\psi_i)\mathbf{s}_{i/\sigma_i} +\\
&\quad \cos(\psi_i)\dot{\mathbf{s}}_{i/\sigma_i} + \cos(\psi_i)\dot{\psi}_{i/\sigma_i}\mathbf{z}_i - \dot{\psi}_i\sin(\psi_i)\psi_{i/\sigma_i}\mathbf{z}_i
\end{aligned} \tag{51}$$

The analytical expressions of $\dot{\psi}_{i/\sigma_i}$ and $\dot{\eta}_{/\sigma_i}$ are:

$$\begin{aligned}
\dot{\psi}_{i/\sigma_i} &= 2\frac{\dot{\eta}_{/\sigma_i}}{(1+\eta^2)} - 4\frac{\eta\eta_{/\sigma_i}\dot{\eta}}{(1+\eta^2)^2} - \frac{\left(2\tilde{\alpha}\tilde{\alpha}_{/\sigma_i} - \tilde{\beta}_{/\sigma_i}\right)\left(2\tilde{\alpha}\dot{\tilde{\alpha}} - \dot{\tilde{\beta}}\right)}{4\left(\tilde{\alpha}^2+1-\tilde{\beta}\right)^{3/2}} + \left(2\dot{\tilde{\alpha}}\tilde{\alpha}_{/\sigma_i} + 2\tilde{\alpha}\dot{\tilde{\alpha}}_{/\sigma_i} - \dot{\tilde{\beta}}_{/\sigma_i}\right)\\
\dot{\eta}_{/\sigma_i} &= \frac{\dot{\tilde{\alpha}}_{/\sigma_i}}{2\sqrt{\tilde{\alpha}^2+1-\tilde{\beta}}}
\end{aligned} \tag{52}$$

with terms $\dot{\tilde{\alpha}}_{/\sigma_i}$ and $\dot{\tilde{\beta}}_{/\sigma_i}$ computed as follows.

$$\dot{\tilde{\alpha}}_{/\sigma_i} = \frac{2\left(\mathbf{z}_i\cdot\boldsymbol{\delta}_i\right)\left(\boldsymbol{\delta}_i\cdot\mathbf{s}_{i/\sigma_i}\right)\left(\mathbf{s}_i\cdot\boldsymbol{\delta}_i\right)\left(\dot{\mathbf{s}}_i\cdot\boldsymbol{\delta}_i + \mathbf{s}_i\cdot\dot{\boldsymbol{\delta}}_i\right)}{\left(\mathbf{s}_i\cdot\boldsymbol{\delta}_i\right)^4} - \frac{\left(\left(\mathbf{z}_i\cdot\dot{\boldsymbol{\delta}}_i\right)\left(\dot{\mathbf{s}}_i\cdot\boldsymbol{\delta}_i\right) + \left(\mathbf{z}_i\cdot\dot{\boldsymbol{\delta}}_i\right)\left(\boldsymbol{\delta}_i\cdot\dot{\mathbf{s}}_{i/\sigma_i} + \dot{\boldsymbol{\delta}}_i\cdot\mathbf{s}_{i/\sigma_i}\right)\right)\left(\mathbf{s}_i\cdot\boldsymbol{\delta}_i\right)^2}{\left(\mathbf{s}_i\cdot\boldsymbol{\delta}_i\right)^4} \tag{53}$$

$$\dot{\tilde{\beta}}_{/\sigma_i} = 2\tilde{r}\frac{\left(\boldsymbol{\delta}_i\cdot\mathbf{s}_{i/\sigma_i}\right)\left(\dot{\mathbf{s}}_i\cdot\boldsymbol{\delta}_i + \mathbf{s}_i\cdot\dot{\boldsymbol{\delta}}_i\right) - \left(\boldsymbol{\delta}_i\cdot\dot{\mathbf{s}}_{i/\sigma_i} + \dot{\boldsymbol{\delta}}_i\cdot\mathbf{s}_{i/\sigma_i}\right)\left(\mathbf{s}_i\cdot\boldsymbol{\delta}_i\right)^2}{\left(\mathbf{s}_i\cdot\boldsymbol{\delta}_i\right)^4} \tag{54}$$

References

[1] A. Trevisani, Underconstrained planar cable-direct-driven robots: a trajectory planning method ensuring positive and bounded cable tensions, Mechatronics 20 (2010) 113–127, https://doi.org/10.1016/J.MECHATRONICS.2009.09.011.

[2] Z. Zhang, Z. Shao, Z. You, X. Tang, B. Zi, G. Yang, C. Gosselin, S. Caro, State-of-the-art on theories and applications of cable-driven parallel robots, Front. Mech. Eng. 17 (2022), https://doi.org/10.1007/s11465-022-0693-3.

[3] J. Bettega, G. Piva, D. Richiedei, A. Trevisani, Model predictive control for path tracking in cable driven parallel robots with flexible cables: collocated vs. noncollocated control, Multibody Syst. Dyn. (2023), https://doi.org/10.1007/s11044-023-09881-0.

[4] A. Zahedi, A.M. Shafei, M. Shamsi, On the dynamics of multi-closed-chain robotic mechanisms, Int. J. Non Lin. Mech. 147 (2022) 104241, https://doi.org/10.1016/J.IJNONLINMEC.2022.104241.

[5] R.L. Williams, P. Gallina, J. Vadia, Planar translational cable-direct-driven robots, J. Rob. Syst. 20 (2003), https://doi.org/10.1002/rob.10073.

[6] H. Marufkhani, M.A. Khosravi, Robust optimal constrained control of fully-constrained cable-driven parallel robots based on GSDRE, Nonlinear Dynam. (2023), https://doi.org/10.1007/s11071-023-08693-3.

[7] E. Idà, T. Bruckmann, M. Carricato, Rest-to-Rest trajectory planning for underactuated cable-driven parallel robots, IEEE Trans. Robot. 35 (2019) 1338–1351, https://doi.org/10.1109/TRO.2019.2931483.

[8] P. Bosscher, R.L. Williams, L.S. Bryson, D. Castro-Lacouture, Cable-suspended robotic contour crafting system, Autom. ConStruct. 17 (2007), https://doi.org/10.1016/j.autcon.2007.02.011.

[9] A. Arena, E. Ottaviano, V. Gattulli, Dynamics of cable-driven parallel manipulators with variable length vibrating cables, Int. J. Non Lin. Mech. 151 (2023) 104382, https://doi.org/10.1016/J.IJNONLINMEC.2023.104382.

[10] E. Ottaviano, A. Arena, V. Gattulli, Geometrically exact three-dimensional modeling of cable-driven parallel manipulators for end-effector positioning, Mech. Mach. Theor. 155 (2021) 104102, https://doi.org/10.1016/J.MECHMACHTHEORY.2020.104102.

[11] T.K. Mamidi, S. Bandyopadhyay, A computational framework for the dynamic analyses of cable-driven parallel robots with feed and retrieval of cables, Mech. Mach. Theor. 186 (2023) 105338, https://doi.org/10.1016/J.MECHMACHTHEORY.2023.105338.

[12] S. Behzadipour, A. Khajepour, Time-optimal trajectory planning in cable-based manipulators, IEEE Trans. Robot. 22 (2006), https://doi.org/10.1109/TRO.2006.870663.

[13] T. Heyden, C. Woernle, Dynamics and flatness-based control of a kinematically undetermined cable suspension manipulator, Multibody Syst. Dyn. 16 (2006) 155–177, https://doi.org/10.1007/s11044-006-9023-5.

[14] T.K. Mamidi, S. Bandyopadhyay, Forward dynamic analyses of cable-driven parallel robots with constant input with applications to their kinetostatic problems, Mech. Mach. Theor. 163 (2021) 104381, https://doi.org/10.1016/J.MECHMACHTHEORY.2021.104381.

[15] P. Tempel, A. Schmidt, B. Haasdonk, A. Pott, Application of the rigid finite element method to the simulation of cable-driven parallel robots, in: Mechanisms and Machine Science, 2018, https://doi.org/10.1007/978-3-319-60867-9_23.

[16] G. Boschetti, F. González, G. Piva, D. Richiedei, B. Rodríguez Frade, A. Trevisani, Synthesis of an extended Kalman Filter for cable-driven parallel robots. https://doi.org/10.3311/eccomasmbd2021-199, 2021.

[17] J. García De Jalón, Twenty-five years of natural coordinates, Multibody Syst. Dyn. 18 (2007) 15–33, https://doi.org/10.1007/s11044-007-9068-0.

[18] J. García de Jalón, Kinematic and Dynamic Simulation of Multibody Systems the Real-Time Challenge, 1994.
[19] P. Flores, Concepts and Formulations for Spatial Multibody Dynamics, Springer, 2015.
[20] D. Gan, S. Caro, G. Chen, S. Nokleby, J.S. Dai, Special section: Theory and design of reconfigurable mechanisms and robots, J. Mech. Robot. 14 (2022), https://doi.org/10.1115/1.4055836.
[21] J. Bettega, G. Boschetti, G. Piva, D. Richiedei, A. Trevisani, Reconfiguration strategy for fully actuated translational cable-suspended parallel robots, Front Robot AI 10 (2023), https://doi.org/10.3389/frobt.2023.1112856.
[22] C. Gosselin, Global planning of dynamically feasible trajectories for three-dof spatial cable-suspended parallel robots, in: Mechanisms and Machine Science, 2013, pp. 3–22, https://doi.org/10.1007/978-3-642-31988-4_1.
[23] M. Stoltmann, P. Froitzheim, N. Fuchs, C. Woernle, Flatness-based feedforward control of a crane manipulator with four load chains. https://doi.org/10.1007/978-3-319-98020-1_8, 2019.
[24] P. Tempel, A. Verl, A. Pott, On the dynamics and Emergency Stop behavior of cable-driven parallel robots. https://doi.org/10.1007/978-3-319-33714-2_48, 2016.
[25] C.M. Pappalardo, A natural absolute coordinate formulation for the kinematic and dynamic analysis of rigid multibody systems, Nonlinear Dynam. 81 (2015) 1841–1869, https://doi.org/10.1007/s11071-015-2111-4.
[26] X.M. Xu, J.H. Luo, X.G. Feng, H.J. Peng, Z.G. Wu, A generalized inertia representation for rigid multibody systems in terms of natural coordinates, Mech. Mach. Theor. 157 (2021), https://doi.org/10.1016/j.mechmachtheory.2020.104174.
[27] C. Kraus, M. Winckler, H.G. Bock, Modeling mechanical DAE using natural coordinates, Math. Comput. Model. Dyn. Syst. 7 (2001) 145–158, https://doi.org/10.1076/mcmd.7.2.145.3645.
[28] Z. Zhang, G. Xie, Z. Shao, C. Gosselin, Kinematic Calibration of cable-driven parallel robots considering the pulley kinematics, Mech. Mach. Theor. 169 (2022) 104648, https://doi.org/10.1016/J.MECHMACHTHEORY.2021.104648.
[29] J.C. Santos, M. Gouttefarde, in: J. Lenarčič, B. Siciliano (Eds.), A Real-Time Capable Forward Kinematics Algorithm for Cable-Driven Parallel Robots Considering Pulley Kinematics - Advances in Robot Kinematics 2020, Springer International Publishing, Cham, 2021, pp. 199–208.
[30] P. Tempel, P. Miermeister, A. Pott, Kinematics and dynamics modeling for real-time simulation of the cable-driven parallel robot IPAnema 3, in: Proceedings of the 14th IFToMM World Congress, 2015, pp. 117–123.